Center for Electromechanics

The University of Texas at Austin

College of Engineering • Bureau of Engineering Research
Taylor Hall 167 • Austin, Texas 78712 • 512-471-4496

A STUDY PERTAINING TO INERTIAL ENERGY STORAGE MACHINE DESIGNS FOR SPACE APPLICATIONS

FINAL REPORT

August 1981

Submitted to
Jet Propulsion Laboratory
Contract No. 955969

Written by
Raymond C. Zowarka

Center for Electromechanics
Taylor Hall 167
The University of Texas at Austin
Austin, Texas 78712

Telephone 512/471-4496

ABSTRACT

This report presents the preliminary design of a counterrotating fast discharge homopolar generator (HPG) and a counterrotating active rotary flux compressor (CARFC) for space application. The HPG is a counterrotating spool-type homopolar with superconducting field coil excitation. It delivers a 20-ms, 145-kJ pulse to a magnetoplasmahydrodynamic thruster. The peak output current is 42.7 kA at 240 V. After 20 ms the current is 29.7 kA at 167 V.

The CARFC delivers ten 50-kJ, 250-μs pulses at 50-ms interval to six Xenon flash lamps pumping an Nd glass laser. The flux compressor is counterrotating for torque compensation. Current is started in the machine with a 5-kV, 5-kJ pulse-charged capacitor. Both designs were based upon demonstrated technology, but the sensitivity of the designs to technology that may be available in five to ten years was determined.

CONTENTS

FIGURES

TABLES

INTRODUCTION

From 1973 until the present the Center for Electromechanics at The University of Texas at Austin (CEM-UT) has engaged in the design, fabrication, and testing of pulsed homopolar generators (HPGs). In 1978 CEM-UT designed, constructed, and tested the first compensated pulsed alternator (compulsator). The purpose of this contract is to apply this experience to a preliminary engineering design for an HPG and a compulsator to be used for space applications.

> "It must be kept in mind that the goal of this contract is to do a preliminary engineering design in as much detail as the resources will allow for an HPG and a compulsator to be used for space applications. The load for the HPG will be a pulsed MPD thruster and the load for the compulsator will be a Nd glass laser. These are just candidate loads (applications) and the goal of the contract is not to do a systems design or machine optimization for these loads, but rather to use these candidate loads as examples in order to do a detailed machine design for space applications."

The Contractor shall:

(1) Provide the necessary labor, materials and facilities to conduct a preliminary engineering point design of a Homopolar Generator (HPG) and a Compensated Pulsed Alternator (CPA) to be used in space. The load for the HPG shall be a Magneto Plasma Dynamic (MPD) thruster and the load for the CPA shall be a high power, pulsed laser.

(2) Provide the electrical and operating characteristics of the laser.

(3) Design the HPG and CPA in accordance with their respective state-of-the-art, as well as the requirement to keep the mass of a space system as small as possible.

(4) Develop a technique and/or a design by which the HPG and the CPA can be charged (motored) using a constant input power from the prime power source.

(5) Design the HPG and the CPA so that the uncompensated reaction torque will be minimized.

(6) Calculate the mass, volume and efficiency of the HPG and CPA and estimate the cost and lifetime of each machine.

Minimum mass, maximum efficiency, and minimum uncompensated reaction torque are the key design items. The load for the HPG will be a magnetoplasmadynamic (MPD) thruster. A fast-discharging counterrotating disk-type HPG was selected to provide an output characteristic demonstrating

a fast current rise to 40 kA at 240 terminal volts decaying to 32 kA at 167 terminal volts in 20 ms. This machine will recharge in 2 s drawing constant powers from the prime source. The operating mode will be repetitive discharge every 2 s for a 9-to-12-month mission duration.

The load for the compulsator will be a parallel configuration of six Xenon flash lamps pumping an Nd glass laser. The compulsator will be operated three to four times a day for a one-year mission. The operating mode for the compulsator will be a discharge burst of ten 50-kJ pulses of 200-500-μs half width, one every 50 ms (20 Hz). A counterrotating drum compulsator was designed and on discharge the rotor decelerated to half speed after delivering one 500-μs pulse. With this information the design was changed to a counterrotating active rotary flux compressor (CARFC). This machine stores enough energy to perform in the burst mode. The differences between a compulsator and an active rotary flux compressor (ARFC) will be described in the body of the report. The duty cycle of the CARFC will be a discharge burst three to four times per day.

CEM-UT has designed, constructed, and tested a noncounterrotating ARFC of the size proposed in this contract. Design codes are complete and match experimental results. An added point of interest is that a desk model compulsator has successfully driven flash lamps in a repetitive mode. (Fig. 1). [1] All of these developments instill confidence in the accuracy of the design and capability of the proposed machine to perform in the repetitive discharge mode.

ORIGINAL PAGE
BLACK AND WHITE PHOTOGRAPH

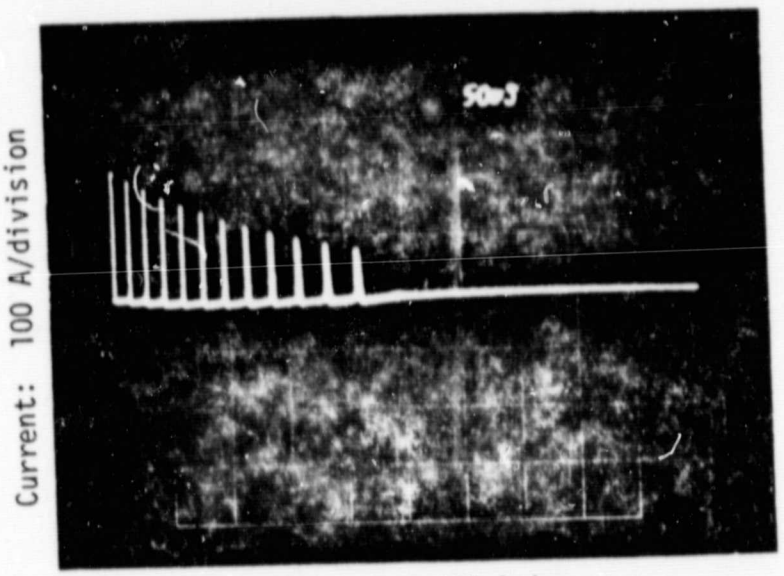

Fig. 1. Repetitive Flash Lamp Discharge

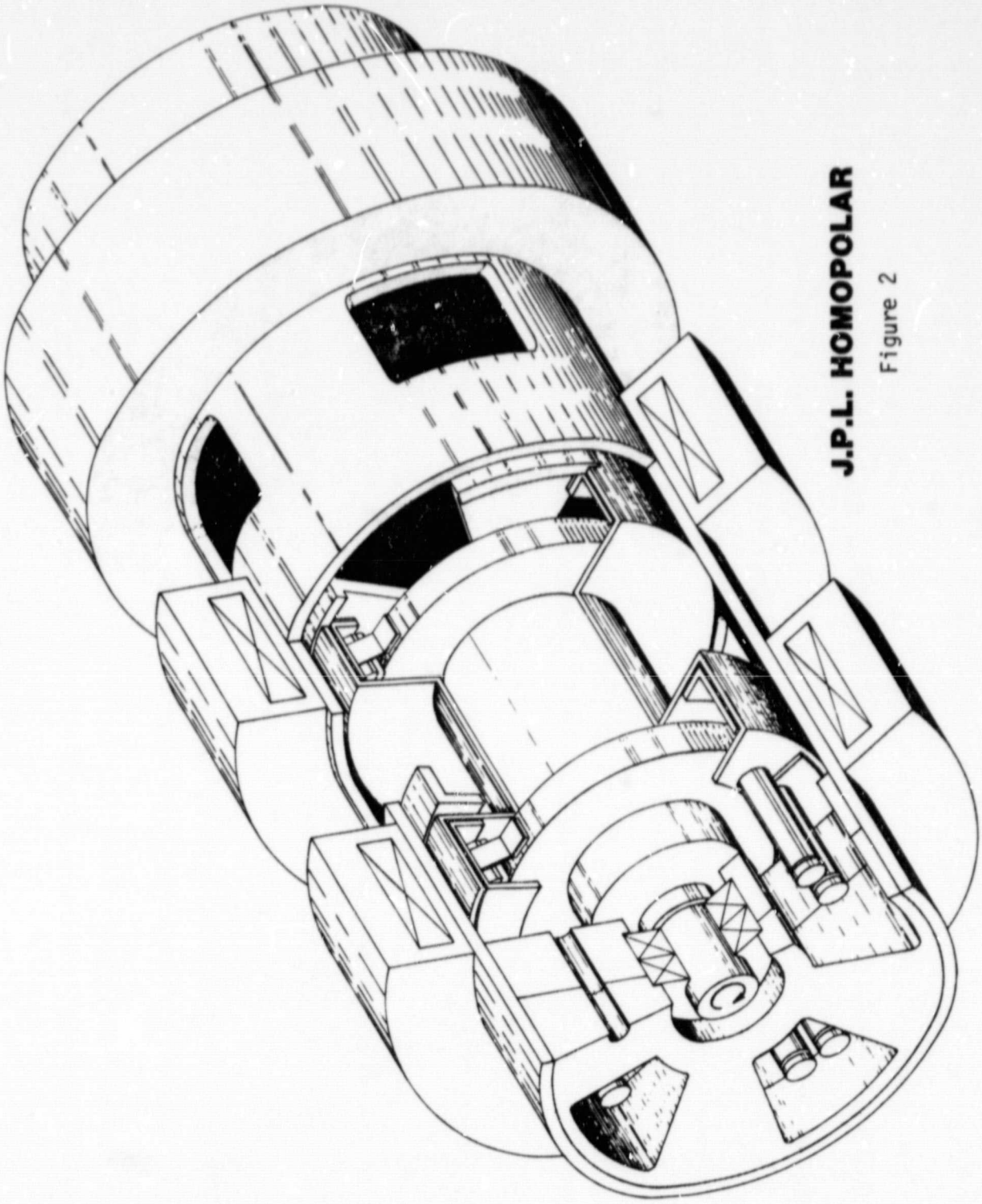

J.P.L. HOMOPOLAR

Figure 2

PRECEDING PAGE BLANK NOT FILMED

DESIGN OF AN HPG TO DRIVE AN MPD LOAD

HPG Circuit Design

A review of design considerations is appropriate at this point. The circuit is treated as a simple RLC network. The HPG modeled as a capacitor is charged and then its energy is delivered to the thruster load through a making switch S_1 (Fig. 3). The load resistance was computed from nominal voltage/current characteristics for a Princeton/JPL MPD arc with a gas flow of 6 g/s argon. [2] The initial voltage and current are 240 V @ 40 kA and after a pulse length of 20 ms, the voltage and current will be 167 V @ 32 kA, indicating an average resistance of 5.61 mΩ. These parameters were established in a March 10 meeting between CEM-UT and JPL and later confirmed in a March 15 letter from Ross Jones to CEM-UT. These operating parameters are entering the fast discharge regime for HPGs. For this reason disk-type HPGs will be considered in this point design. [3]

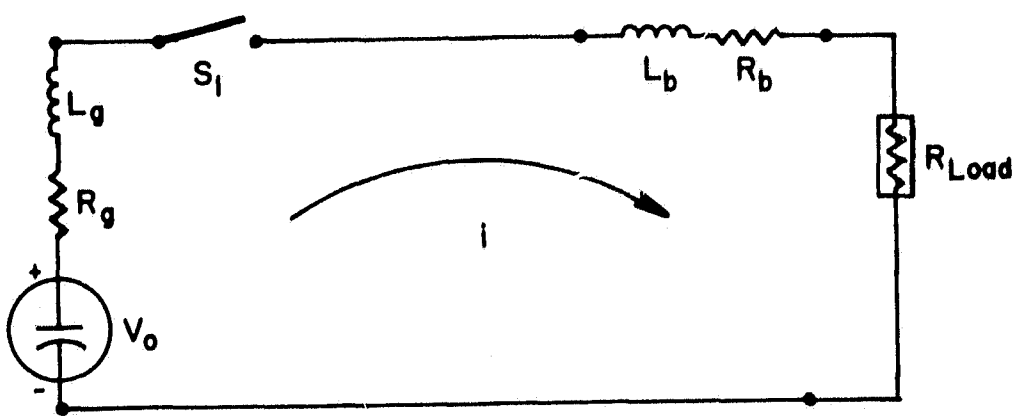

Fig. 3. Simplified HPG Circuit Diagram

The switching in this circuit is not a trivial matter. The arc must be initiated in the thruster. The HPG must then be switched in to provide follow-on current. Next the arc must be extinguished and the HPG making switch must be opened. If the insulation on the HPG must be designed to operate significantly above generator open circuit voltage levels, it will have a significant effect on the machine design. This must be kept in mind when the switching is designed.

The solution of the network in Figure 3 along with the boundary conditions supplied by JPL lead to the following equations:

$$i(t_1) = \frac{V_o}{\left[\left(\frac{1}{2\ L/R}\right)^2 - \frac{1}{LC}\right]^{1/2} L} e^{-\frac{t_1}{2\ L/R}} \sinh\left[\left(\frac{1}{2\ L/R}\right)^2 - \frac{1}{LC}\right]^{1/2} t_1 \quad (1)$$

t_1, V_o, and C are unknowns.

$$i(t_2) = \frac{V_o}{\left[\left(\frac{1}{2\ L/R}\right)^2 - \frac{1}{LC}\right]^{1/2} L} e^{-\frac{t_2}{2\ L/R}} \sinh\left[\frac{1}{2\ L/R^2} - \frac{1}{LC}\right]^{1/2} t_2 \quad (2)$$

t_2, V_o, and C are unknowns.

$$t_1 = \tanh^{-1} \frac{\left(2\left[\left(\frac{1}{2\ L/R}\right)^2 - \frac{1}{LC}\right]^{1/2} L/R\right)}{\left[\left(\frac{1}{2\ L/R}\right)^2 - \frac{1}{LC}\right]^{1/2}} \quad (3)$$

In this equation t_1 is related to C and from the operating conditions, $t_2 - t_1 = 0.020$ s, t_1 is related to t_2. The only unknowns remaining at this point are V_o and C. A computer program was written to vary V_o and

C until equations 1 and 2 were satisfied. The equivalent capacitance of the homopolar will be 8.9 F. The open circuit voltage before discharge will be 266 V.

The expression for the homopolar voltage is

$$\frac{V_o}{n} = \frac{\omega\phi}{2\pi} . \tag{4}$$

V_o = open circuit voltage (V)
n = number of rotors
ω = angular speed (rad/s)
ϕ = flux (Wb).

Assuming a uniform flux density across the rotors

$$\phi = B\pi r_o^2 . \tag{5}$$

B = flux density (T)
r_o = rotor outer radius (m).

Equation 5 may be substituted into equation 4 and the angular velocity related to the surface speed to produce equation 6.

$$B = \frac{2V_o}{nvr_o} \tag{6}$$

v = rotor surface speed (m/s)

The stored inertial energy is equated to the energy in the capacitor by

$$nJ\omega^2 = CV_o^2 \tag{7}$$

J = mass moment of inertia
C = equivalent capacitance.

Substituting the expression for the mass moment of inertia of a disk into

equation 7, and requiring the disk thickness to be 0.2 r for dynamic considerations, yields

$$r_o^3 = \frac{2CV_o^2}{0.2\ n\pi\rho v^2} . \qquad (8)$$

ρ = density of the rotor material (kg/m^3).

277 m/s was selected as a representative surface speed. This value was the proposed surface speed for a fast-discharging HPG designed in a joint effort between The University of Texas at Austin, Los Alamos National Scientific Laboratory, and Westinghouse Research Laboratories in 1976. [4] Out of that program CEM-UT developed a high speed brush tester; results of that effort are reported later under the brush design section of this report. A surface speed of 277 m/s is substituted into equation 8 and n is varied over the even numbers to meet the torque compensation requirement for space applications. The value of the rotor radius determined by equation 8 is placed in equation 6 to examine the required flux density of the homopolar magnet system. (Table 1.) A four-disk machine requires an average flux density of 3.58 T across the rotors. This value has been realized in operational superconducting magnet systems.

The above study suggests a four-disk machine with counterrotation for torque compensation. CEM-UT has reported on counterrotating spool homopolars [5] and has constructed an experimental fast-discharge HPG (FDX) [6] to model the counterrotating disk portion of the spool machine. The insight acquired in building and testing that machine is applied in the generation of this point design.

HPG Design

HPGs use electromechanical conversion to transform the spinning inertial energy of a rotor into a high energy electrical pulse. It is a well-known law of physics that as a conductor moves in a magnetic field a voltage is induced in the conductor. It is the spool-shaped rotors in this machine that spin thereby cutting flux lines (Fig. 4). A potential difference is created between the periphery of the disk at the end of the spool and the central shaft. The combination of disks and shaft defines

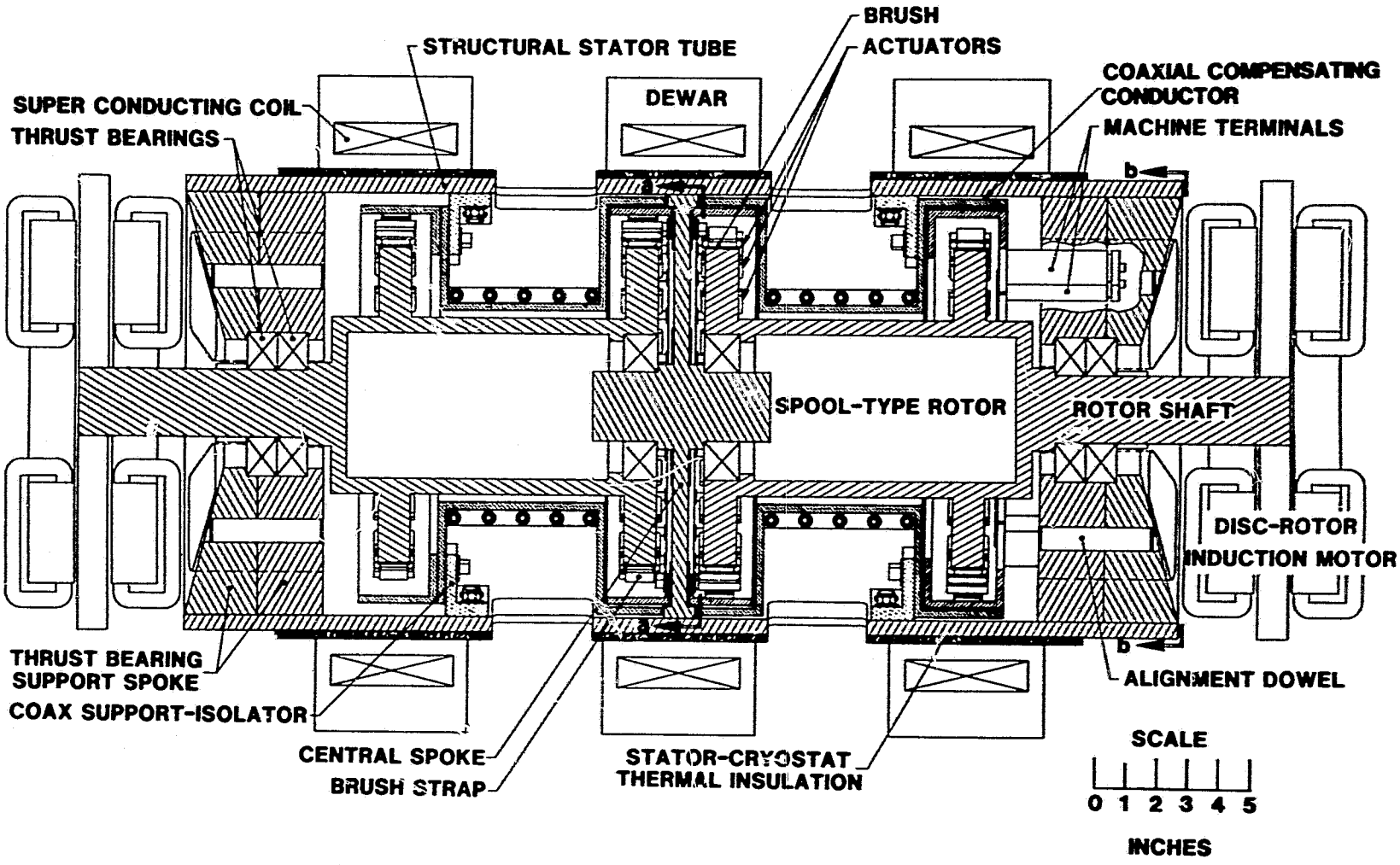

Fig. 4. Cross Section of Counterrotating Spool-type HPG

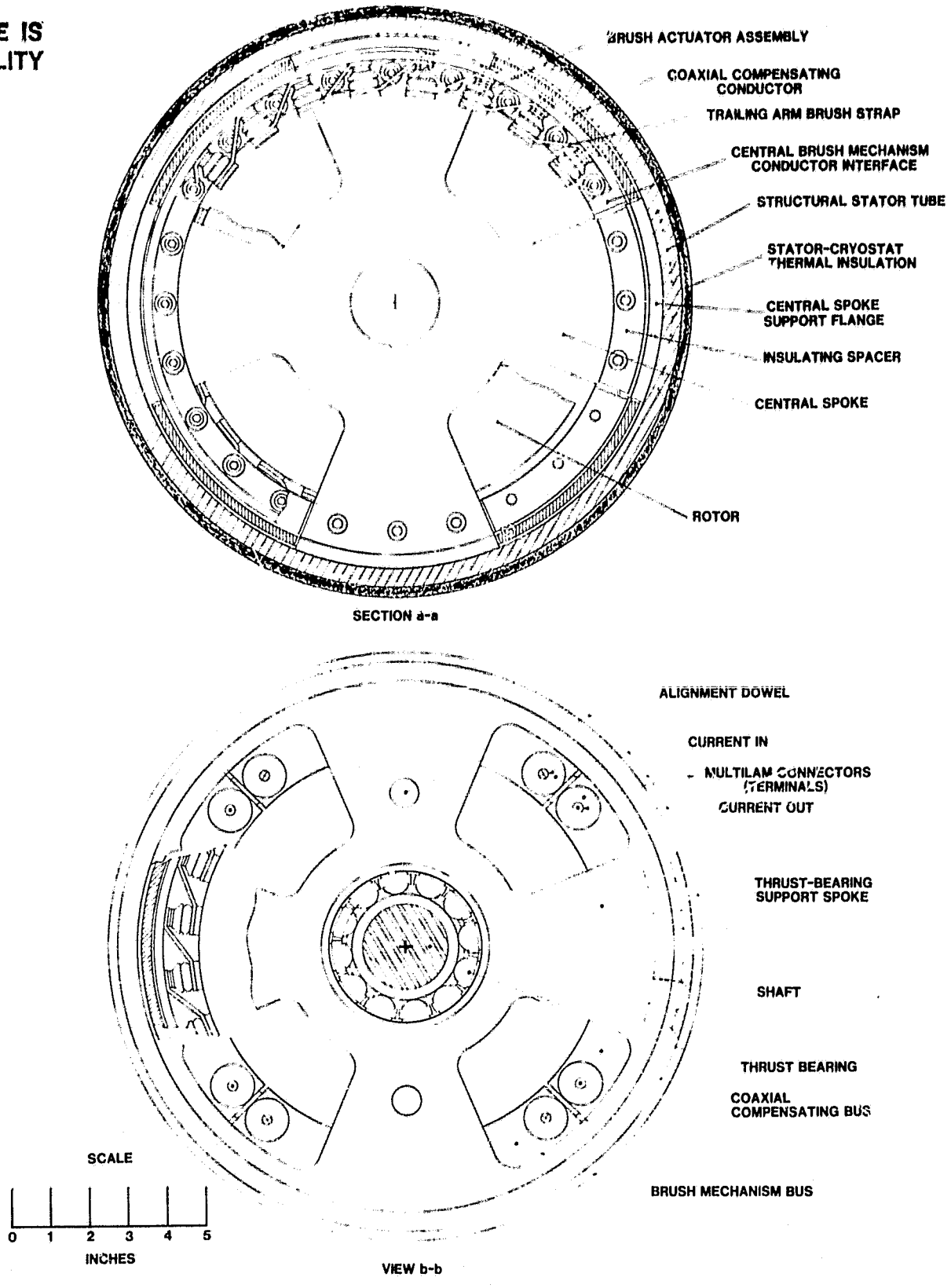

Fig. 5. Thrust Bearing Support Structure and Machine Terminals (view b-b) and Central Bearing Support Structure and Brush Mechanism Cutaway (section b-b)

TABLE 1

CANDIDATE HPG CONFIGURATIONS

No. of rotors	Radius of each rotor (inches)	Mass of each rotor (kg)	$\bar{B}$ (Tesla)	t_1 (msec)	V_{load} voltage at time t_1 secs (volts)	I_{t_1} current at time t_1 (kA)	t_2 (msec)	V_{load} voltage at time t_2 secs (volts)	I_{t_2} current at time t_2 secs (kA)	W_{load} del. energy t_1 to t_2 secs (kJ)	$\frac{W_{load}}{\text{mass of rotors}}$ (kJ/kg)
1	8.38	16.46	9.03	0.53	240	42.79	20.53	167	29.77	145.5	8.84
2	6.65	8.23	5.63	0.53	240	42.79	20.53	167	29.77	145.5	8.84
4	5.28	4.115	3.58	0.53	240	42.79	20.53	167	29.77	145.5	8.84
6	4.61	2.743	2.73	0.53	240	42.79	20.53	167	29.77	145.5	8.84
8	4.19	2.058	2.25	0.53	240	42.79	20.53	167	29.77	145.5	8.84

the spool geometry. In this machine a dc voltage that alternates polarity from one disk to the next is established by rotating the two spools in opposite directions and by making the current direction in the outside field coils opposite to the direction of current in the central field coil.

Consideration of spin stresses in the rotor material determines the angular velocity at which the rotor may spin. Sliding electrical contacts, or brushes, carry the transport current between the moving and stationary parts of the machine. The maximum sliding velocity of the brush is determined by thermal considerations. This surface velocity limit along with the required angular velocity set the rotor diameter.

The rotor periphery must be very close to the inner diameter of the field coils to maximize flux linkage. The coils will be superconducting for economy of weight and excitation power. An average flux density of 4 T is realized in many present day superconducting magnet systems. This design will use a value of average flux density below 4 T.

> "The main requirement of the sliding electrical contacts is that they must be able to follow the collector with enough force to prevent sparking. Secondary requirements are that temperature reached in current carrying members must be acceptable and all forces generated must be suitably restrained." [7]

The brush design for this machine will use trailing arm brushes pressed onto the rotor surface with pneumatic actuators. The brushes must demonstrate wear rates that allow millions of pulses to be taken from the machine over its lifetime.

The stationary portion of the electrical discharge path through this machine is called the compensating conductor. It conforms to the rotor profile so that the area between the current path through the rotors and the return through the compensating turn is kept small. Therefore, the machine internal inductance is minimized. This will allow for fast current rise times and fast discharges as required in the MPD thruster application. This conductor design also features bayonet removable connectors at the machine busbar termination, which will allow easy mating of the power supply to the load.

The rotor support structure of the machine is called the stator. The bearings support the rotors from this structure. The total structure is designed to have radial and axial stiffness sufficient to allow

operation of the machine safely below any critical frequencies of the system. This structure also supports the nonrotating electrical members and sustains the reaction torque between the two rotors during discharge. The design of the stator requires that the axis of the two rotors coincide to very close tolerances in order to minimize uncompensated reaction torque. Also the brush mechanisms supported from this structure must center accurately on the rotor slip rings.

The final member of the homopolar system is the prime mover. The drive must supply enough power to take the rotors to design speed at the desired repetition rate of the system. In this design it is required that the motoring system utilize a constant power input of 100 kW. Because the installation is not serviceable the most reliable mode of operation is to leave the drive hard coupled to the homopolar rotors. Under this requirement the inertia of the drive must be kept small in order that the rotor to motor coupling can withstand the discharge torque.

HPG Operating Procedure

The superconducting field coils will be excited with a programmed power supply. Once field is established the prime movers will utilize constant power from the solar panel to bring the inertia to speed in 2 s. At this point the discharge circuit will be interrogated and if the logic is satisfied pneumatic actuators will push the brushes against the rotor surface. Once the arc is established in the thruster the making switch will close and the HPG will discharge into the thruster. If the HPG controller receives the making switch open command, the brushes will retract and the prime movers will repower to take the inertia back to full speed. If the switching does not occur, the brushes will remain down and the total stored energy will be delivered to the load. Interrogation of the switching system will then control system restart.

Field Coil Design

The magnet system for the HPG excitation was modeled closely from a split pair superconducting magnet system for self-colliding beam experiments (MIGMA). [8] This magnet was chosen because the coil separation and

diameter are very similar to those required by the HPG. (Table 2.)

TABLE 2
MAGNET SPECIFICATIONS

	MIGMA	JPL Homopolar Magnet
Type	Split pair	2 split pairs
Central field	40 kg	35.8 kg
Winding midplane separation	152 mm	134 mm (5.3 in.)
Design current	120 A	300 A
Current density	16,700 A/cm^2*	37,000 A/cm^2
Stored energy	500 kJ	68 kJ/coil
Inside diameter	254 mm	411 mm (16.2 in.)
Outside diameter	668 mm	412 mm (18.2 in.)
Width	76 mm	101 mm (4 in.)
Turns per coil	8,150	1,447
Charging time	30 min	30 min

*Actual magnet current density is 11,000 A/cm^2.

After the rotor brush mechanisms and compensating conductor were laid out, the field coils were sized (Fig. 4). Attention was given to dewar size requirements and the second column of Table 2 reports the coil dimensions.

The coil stored energy is given by

$$E = (\text{Bore area})(\text{Bore length})\frac{B^2}{2\mu_o} = 68{,}000 \text{ J}. \tag{9}$$

The current density is related to the stored energy by the relationship

$$EJ^r = C. \tag{10}$$

Bruchna [9] gives values of 2.5 for r and 1.8×10^{26} for C in MKS units. These values, which are judged to be conservative, give:

$$J = 3.7 \times 10^4 \text{ A/cm}^2. \tag{11}$$

Analysis of the MIGMA magnet yields an attractive force of 489,000 N and a peak tangential stress of 9,479 N/cm^2 (13,757 psi). The coils are impregnated with epoxy resin to prevent movement of individual windings. The epoxy system must be chosen to insure compatibility of thermal coefficients of expansion with the superconductor. Relative motion between the coil winding and coil form is unavoidable. Careful attention must be paid to limited precompression and careful control of radial clearances will insure gradual coil movements. Careful mechanical design will avoid friction-induced hot spots.

For a multiple coil system it is possible for one coil to quench and absorb the stored energy of the three coils,

> "Computer codes exist that follow the spread of resistance within a coil and predict the hot spot growth. The codes will consider a quench to start at any location and will follow its propagation in three dimensions with temperature dependent properties such as heat capacities, thermal conductivity, and resistivity." [8]

The coils can be designed to be self-protecting. The copper-to-superconductor ratio can be specified so that the maximum temperature generated at a quench site will not damage the coil material. Also the coils may be designed so that the voltages generated by a quench will be held to a safe level. Self-protection leads to a simpler electrical system and a more reliable coil design.

In the MIGMA magnet the system weight per cryostat is 682 kg.

Rotors

Each of two rotors will be fabricated in a spool design from a single 7050 aluminum forging. The rotors have an individual moment of inertia of 0.091 $J\text{-}s^2$. The rotor mass is 11.1 kg. The rotor speed is

$$\omega = \frac{v}{r} = 2065 \frac{\text{rad}}{\text{s}} \quad (20{,}000 \text{ rpm}) \tag{12}$$

The peak radial stress in the rotor disk is given by

$$s_r = \rho\omega^2 \frac{3+\mu}{8} (r_o^2 + r_i^2 - 2 r_o r_i) \tag{13}$$

$$= 2.8 \times 10^7 \frac{nt}{m^2} (4{,}022 \text{ psi})$$

where

s_r = peak radial stress
ρ = material density
ω = angular speed
r_o = outer radius of the disk
r_i = inner radius of the disk
μ = Poisson's ratio.

The peak tangential stress in the rotor disk occurs at the inner radius and is given by

$$s_t = \rho\omega^2 \frac{3+\mu}{8} (2r_o^2 + (1 - \frac{1+3\mu}{3+\mu})r_i^2) \tag{14}$$

$$= 1.9 \times 10^8 \frac{nt}{m^2} (27{,}200 \text{ psi})$$

s_t = peak tangential stress.

The outer periphery of the rotors will be flame sprayed with a copper coating. This will provide a surface for the brushes to run on. Both voltage drop and wear considerations are influenced by this selection.

Compensating Turns and Output Design

The stator conductors are designed to closely follow the rotor contour to insure a low circuit inductance and total output current compensation. The compensating turns are split right circular cylinders that bolt along an axial seam to enclose the rotors. There is one bolted joint in the bus bar for assembly purpose and radial windows are provided in the bearing support tube between cryostats for machine assembly. The output connectors

are bayonet-type connectors with Multilam R type LA1/.25 spring contact fingers (see Fig. 6). This connector allows for convenient bus termination. If flexible cables are required to bolt into the thruster housing, the cable may be swaged into the connectors. If coaxial transmission is desired the coaxial output tubes may be silver brazed to the connectors and easily plugged into the end of the machine. This contact has been tested in the CEM-UT laboratory and has a 3 s, 44 kA pulse rating. The total stator conductor weight is 63 kg (139 lbs).

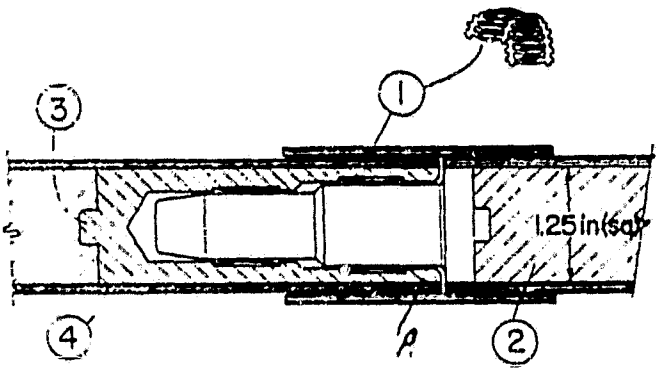

Fig. 6. Contact Plug

1. Contact spring
2. Conductor
3. Brazed joint
4. Coil insulation

Brush System Design

> "The main requirement is that the brushes must be able to follow the collector surface and must be held onto the collector with enough force to prevent sparking. Secondary requirements are that temperatures reached in current carrying members must be acceptable and all forces generated must be suitably restrained." [7]

In the thruster application the brush system must be able to deliver a large number of pulses without service. Table 3 presents representative data of present brush technology. Most brush test data are collected for long pulses in order that measurable wear is apparent over a reasonable number of pulses. Also brush data for slow discharge homopolars is more prevalent. Wear is highly dependent on brush temperature and 20 ms pulses

TABLE 3

PRESENT BRUSH TECHNOLOGY--REPRESENTATIVE DATA

Reference	Material	Surface Velocity (m/s)	Current per Brush (A)	Wear/Pulse (m)	Pulse Duration (s)
Design of brush gear for high current pulses and high rubbing velocities, R. A. Marshall [10]	CM1S	56	2,800	3.94×10^{-4}	2
Measurement of the friction and wear characteristics of copper graphite sliding electrical contact materials at very high speeds and current densities, J. M. Casstevens [11]	CM1S	155	600	1.52×10^{-4}	60
	CM1S	155	0	4.06×10^{-5}	60
	CM1S	230	0	1.37×10^{-4}	60
Testing and evaluation of brushes used for the fast discharge homopolar generator through the use of the controlled atmosphere brush-testing facility, M. J. Bharucha [12]	CM1S	277	0	5.08×10^{-7}	0.190
	CM1S	146	4,300	2.41×10^{-8}	0.340
An investigation of the tribological properties of graphite fiber-metal matrix composites, C. H. Ramage [13]	Cu 3% Sn HM 3000 Fiber	60	?	2.18×10^{-8}	60

will not raise the brush temperature as a 60 s pulse does. The most representative data for this application is presented by Barucha. This work was performed at CEM-UT for the Electrical Power Research Institute. The brush tester was designed to model a 5,000 A/brush, 30-ms pulse through a sliding contact with a surface speed of 277 m/s. This data predicts a 1/2 in. brush of CM1S copper-graphite composite surviving 2.5×10^6 pulses, the equivalent of 1 pulse every 2 s for 1 mo.

In order to hold the brush against the rotor at high speeds without bouncing, the actuator must have low unsprung mass. The actuator shown in Figures 7 and 8 is presently under test at CEM-UT. The mechanism is an inflatable neoprene bladder molded to a metal support. The actuator provides down forces of 49.5-66.7 nt/brush (10-15 lb/brush) and this particular design allows 0.48 cm (3/16 in.) of total brush travel. This configuration of the air bladder forcing down a trailing arm brush has a response time of 3 ms. The homopolar 2 s cycle time represents a short window. The fast brush actuation will halp the overall system controllability. This design is further desirable for its small radial height. Leakage of field coil flux is minimized with this selection.

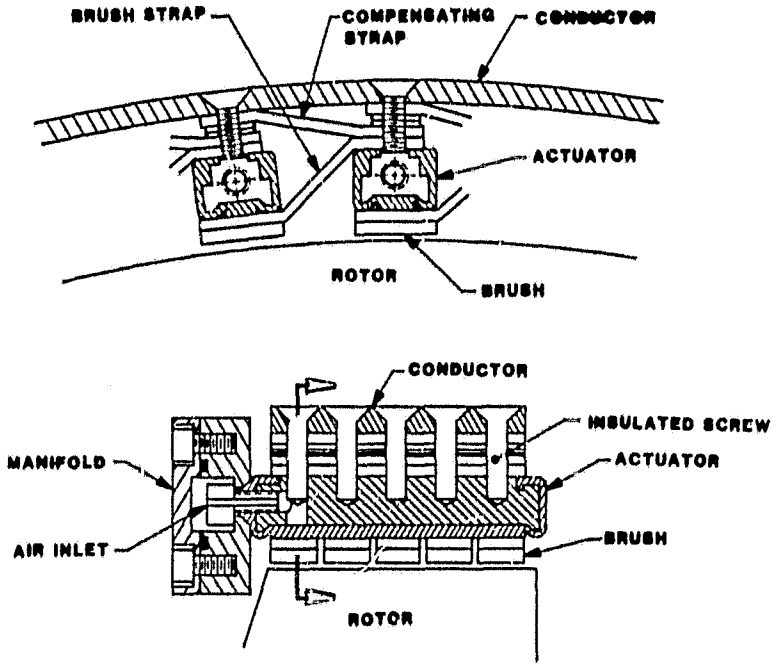

Fig. 7. Brush Actuator

The brushes are spaced around the rotor periphery every 15°. There are then 24 brushes per rotor, giving a peak current per brush of 1,600 A. The brush dimension is 2.21 cm x 1.27 cm (0.87 in. x 0.5 in.).

Further development of present brush technology is required to realize brush wear compatible with the required nine-month operating life. The work performed by Ramage, Table 3, [13] on graphite fiber metal brushes shows promise in that wear rates of this material under long pulse conditions are equivalent to CMIS under short pulse duty. Further testing of this material would be desirable for space application.

Humidity of the atmosphere surrounding the brush has a marked effect on the performance of the graphite as a lubricant, and thus on the friction and wear behavior of the brush. Also, lower oxidation rates may be obtained in less active environments, H_2 or CO_2. Films formed while testing in these environments effectively prevent metal to metal contact between the brush and rotor, thus avoiding high friction and wear. In addition, the large-scale formation of oxide films and the accompanying increase in wear rate do not occur.

As the brushes wear, the brush dust is slung by the motor into the interior of the machine. This material is conductive and must be positively collected. Some work has been done on electrostatic brush dust collection. Other systems--for example, vacuum or directed flow--need to be examined since brush debris collection efficiency is a requirement in the weightlessness of space. Another system needing further development is the actuator design that must show a lifetime of 10^7 of cycles.

Bearings and Structure

For subcritical operation the rotor support system must show an overall stiffness, k, in excess of

$$k \geq \omega^2 m \quad (15)$$

$$\geq \left(2065 \frac{\text{rad}}{\text{s}}\right)^2 \quad 11.1 \text{ kg}$$

$$\geq 4.7 \times 10^7 \text{ nt/m}$$

where m is the mass of the rotor.

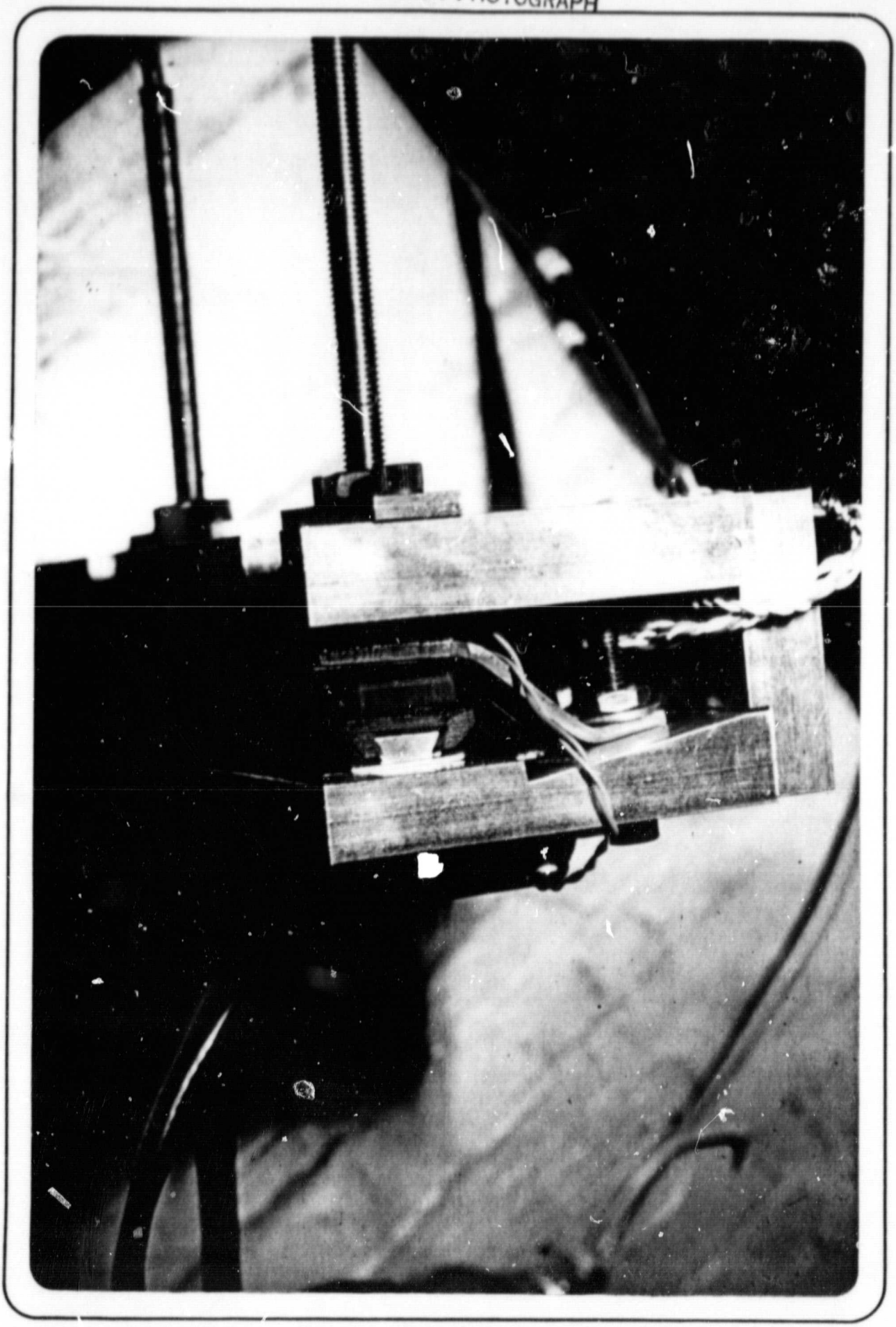

Fig. 8. Brush Actuator

Because the bearings are in a series mechanical path to ground they must exhibit a stiffness greater than this value. An angular contact pair is chosen to supply axial stiffness and a cylindrical rolling element bearing supports the rotor from the central spider to provide radial stiffness. The bearing dimensions used in Figure 4 are catalog specifications for metal bearings of the above types. Metal rolling element bearings cannot be used in this application because more than 100 mV of homopolar voltage will be generated across the bearing. The bearings are rotating in a high field region of the machine and therefore potential difference is generated across moving parts. This voltage leads to arc induced pitting and accelerated wear in the bearing. This part of the design requires utilization of the five to ten year time span for technological development. It is assumed that ceramic rolling element bearings capable of the larger angular velocities will be available. Also assumed is that the size of the ceramic bearing package will be similar to their metal counterparts.

Hydrostatic and hydrodynamic bearings may still be considered, but handling the large oil flow rates in space is difficult.

> "Peculiarities of space environment contribute to the friction and bearing problems. For example, the low-pressure environment contributes to rapid evaporation of liquid or semisolid grease lubricants normally employed. Also, the presence of radiation flux can influence the stability of some of these commonly used lubricants. Other problems arise because of the lack of oxygen available at the extremely low pressures of space, since the lubrication function is, with many metals, strongly influenced by the presence or absence of oxide films on these metals. Finally, one of the principal requirements of any mechanism operating in space is that it be completely reliable. For maximum reliability, each of these preceding problems must be examined closely." [14]

Motoring System

For the remote operation in space the 2-s rep rate over the 9 month to 1 year operation, it will probably be required to keep the prime mover hard coupled to the homopolar rotors. The maximum torque the homopolar shaft can transmit is given by

$$T = \frac{\tau_{max} J}{r} \quad , \quad J = \frac{\pi r^4}{2}$$

$$= 9.9 \times 10^6 \text{ nt-m.}$$

The peak angular acceleration is

$$\alpha = \frac{T_{inst}}{J_{HPG}} = \frac{\phi I}{2\pi J_{HPG}}$$

$$= \frac{3.58 \text{ T} \quad 40{,}000 \text{ A}}{2\pi \quad .091 \quad \text{J-s}^2}$$

$$= 2.5 \times 10^5/\text{s}^2 .$$

The maximum allowed moment of inertia of the hard coupled prime mover is then

$$J_{max} = \frac{T}{\alpha} = 0.0255 \text{ nt-m-s}^2 .$$

The rotodynamic machines that meet this requirement are either air turbines or hydraulic turbines. With these devices a compressor drawing constant power or a pump motor drawing constant power can supply power to the turbines. The FDX constructed by the CEM-UT in 1975 used modified gas turbines running on compressed air to motor the rotor inertia. The turbines would develop 68 hp at 25,000 rpm. The moment of inertial of the FDX turbine is 0.0095 nt-m-s^2. The hydraulic turbine is more attractive because of the constant volume of the working fluid. All of the problems associated with lubricants mentioned in the bearing design section apply to the hydraulics of this method.

Another prospective motoring system is the solid disk induction motor. An inverting supply will be necessary to generate the ac power required for this motor. It is felt that a design of the appropriate horsepower can be generated for this application. This motoring system is pictured coupled to the homopolar rotors in Figure 4.

> "The induction motor with an axial air gap and a flat homogeneous disk-rotor shows some performance characteristics that are superior to conventional induction machines. Large rotational speeds and small moments of inertia promise high power densities and small mechanical time constant." [15]

Uncompensated Reaction Torque

Ideally the counterrotating rotors connected electrically in series confirm the HPG discharge reaction torque within the HPG stator since net angular momentum is conserved. However, several non-ideal conditions can result in varying amounts of reaction torque being applied to the machine mounting structure. They are

1. imperfect axial or lateral alignment of the rotor disk(s) in the field coil(s) resulting in one rotor cutting more total flux than the other,
2. asymmetry between the outer field coils resulting in one producing more flux than the other,
3. quenching or failure of one outer field coil,
4. development of an alternate current path between the two rotors resulting in more current flowing through one rotor than the other, and
5. unbalanced motoring torque.

Unbalanced motoring torque depends on the ultimate selection of the motoring system to be used and can be addressed by design or careful adjustment and regulation. If necessary, rotor acceleration can be monitored and a feedback control signal generated to balance motoring torque.

Unequal rotor currents would be considered a fault mode and could be addressed by careful attention to the insulation of internal machine conductors. Similarly the quenching or failure of an outer field coil would also be a fault mode which could be addressed by quenching or "dumping" all field coils or at least the other outer field coil in the event that one outer field coil quenches or fails.

Items 1 and 2 result in different rotor disks cutting different total amounts of flux, Φ. Since the discharge torque is given by

$$T = \frac{\Phi I(t)}{2\pi} ,$$

where I is the instantaneous current, the unbalanced reaction torque will simply be proportional to the net difference in flux cut by the two rotors. The approximate sensitivity of the design presented here to these misalignments and/or asymmetrics is given in Table 4.

TABLE 4
APPROXIMATE SENSITIVITY OF UNBALANCED REACTION TORQUES OF PROPOSED HPG TO MISALIGNMENTS AND FIELD-COIL ASYMMETRY

Reaction torque due to asymmetry in field coil flux	6.4×10^3 N·m/Wb
Reaction torque due to axial misaligment of rotor disk in field coil	6.4×10^2 N·m/mm
Reaction torque due to lateral misaligment of rotor disk in field coil	6.4×10^1 N·m/mm

The flux cut by individual rotor disks can be adjusted at assembly by the following techniques:

- axial or lateral adjustment of rotors or coils,
- trimming of individual coils by adjusting excitation current, and
- adjustment of flux by the use of trim coils.

Long-term integration of small unbalanced reaction torque effects might be avoided by periodically reversing the rotation direction of the two rotors.

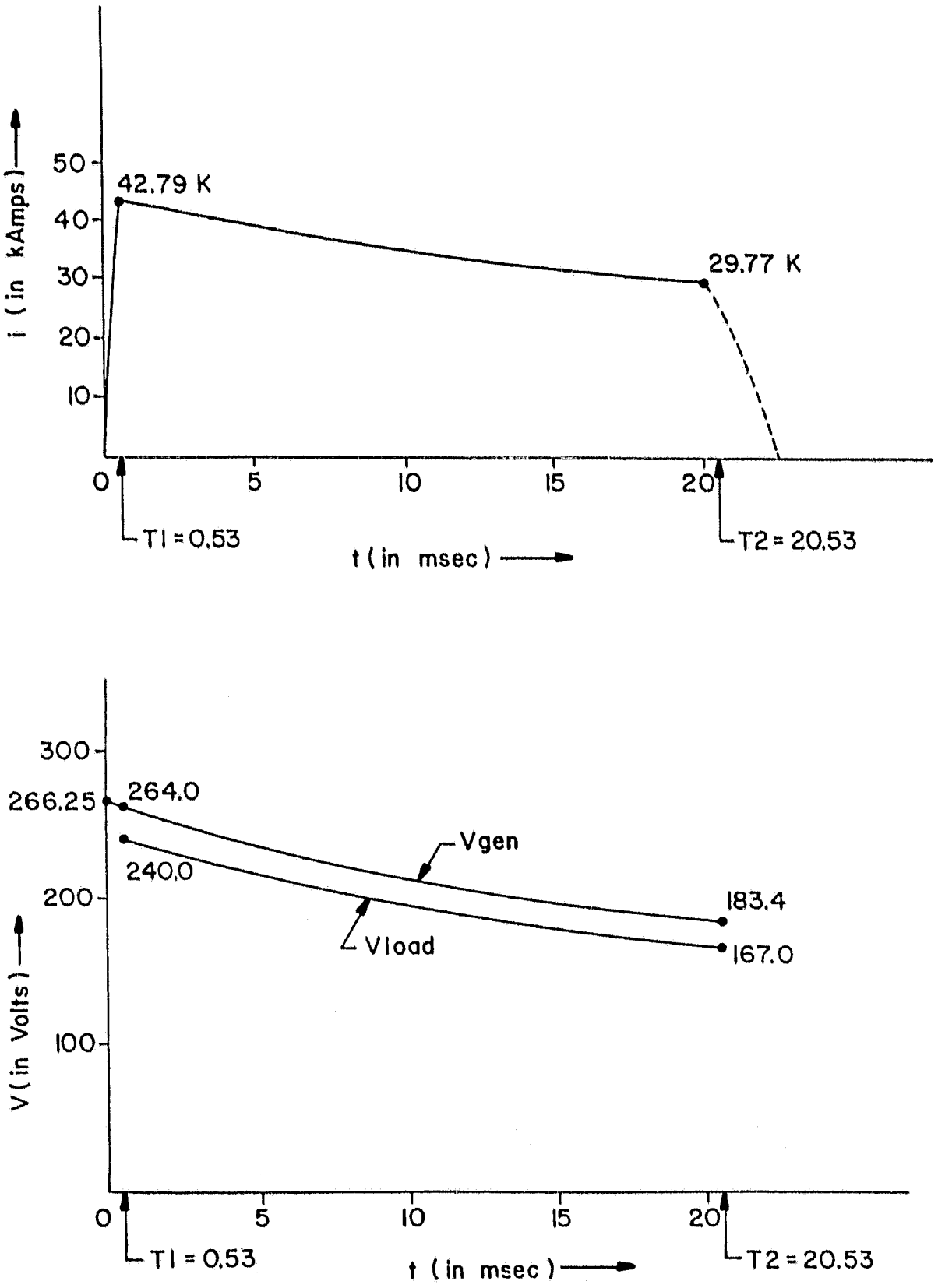

Fig. 9. HPG Driving MPD Thruster (current and voltage)

TABLE 5

JPL HPG CIRCUIT PARAMETERS AND OUTPUT CHARACTERISTICS

Machine Element	Resistance (Ω)	Inductance (H)
4 rotor disks	2×10^{-6}	0.045×10^{-7}
2 rotor drums	5.4×10^{-6}	11.8×10^{-7}
4 compensating disks	2.7×10^{-6}	0.011×10^{-7}
2 end brush collectors	0.35×10^{-6}	-
1 rotor transfer brush collector	0.37×10^{-6}	3.85×10^{-7}
2 compensating drums	1.75×10^{-6}	0.68×10^{-7}
1 compensating drum over rotor transfer brush collector	0.38×10^{-6}	0.018×10^{-7}
1 compensating drum over lead in brush mechanism	0.23×10^{-6}	0.01×10^{-7}
brush straps, 24 around in parallel, 4 sets in series	3.02×10^{-6}	
brush contact drop	89.0×10^{-6}	
2 gap inductances between end rotor disk and compensating disk		0.06×10^{-7}
2 gap inductances between rotor drum and compensating drum		0.025×10^{-7}
2 gap inductances between center rotors and compensating disks		0.04×10^{-7}
1 gap inductance between rotors		0.053×10^{-7}
	105×10^{-6}	16×10^{-7}

JPL Homopolar Weight

	kg	lb
Magnet system	1,758	3,853
Rotors	21.4	46.9
Bearing & structure	114	46.9
Compensating turns & outputs	63	139
Brush system	75	166
Motoring system Disk induction motor	101.4	220
	2,133	4,674

Estimated JPL Homopolar Cost

Price of finished component	K$
Iron shield @ 1.62/lb	4.3
S. C. magnet @ $50/lb	224
Stator conductor @ $8/lb	1.1
Rotor @ $9/lb	0.046
Current collection @ $50/in.^{2}	2.1
Bearings, structure	10
Motoring system	20
Controls	15
	276

System Volume

$$V = \pi(13 \text{ in.})^2 \, 68 \text{ in.} \left(\frac{\text{ft}}{12 \text{ in.}}\right)^3 = 21 \text{ ft}^3 = 0.5947 \text{ m}^3$$

System Life

The brush system at this time limits the life of the machine to 1 month of operation. The graphite fiber metal brushes operating in a short pulse mode might extend the lifetime to 10 months with present technology. The brush actuators have not been tested for millions of cycles. If a

problem arises in this area, it is felt that further development of the design will yield the desired lifetime. The bearing system will also affect system life. It is felt that the concurrent development of nuclear turbine generator systems for space application will lend technological insight to the homopolar bearing design. Further research into ceramic rolling element bearings might solidify the design by yielding a system with high reliability and minimum complexity. Work on ceramic rolling element bearings is underway at SKF Corporation, Fedral Mogul Corporation, and Norton Company. [16]

Efficiency

An overall efficiency may not be determined at this time. By definition the efficiency is the energy delivered to the load divided by the energy delivered by the prime power source. The energy delivered to the load in one discharge is 145.5 kJ. The components of energy delivered by the prime power source are listed below.

HPG rotor bearing and seal loss	8 hp	11.93 kJ/2 s
Super conducting coil heat leak	2.25 ℓ/hr liquid helium	37.52 J/2 s
Energy required to take the rotors from 13,585 rpm to 19,723 rpm		165.8 kJ/2 s
Losses in prime mover		Not estimable at this time

If the prime mover is assumed to be 85% efficient, then 209 kJ must be delivered by the prime power source during the 2 s motoring interval. The efficiency is then

$$\frac{145.5}{209.0} = 69.6\% .$$

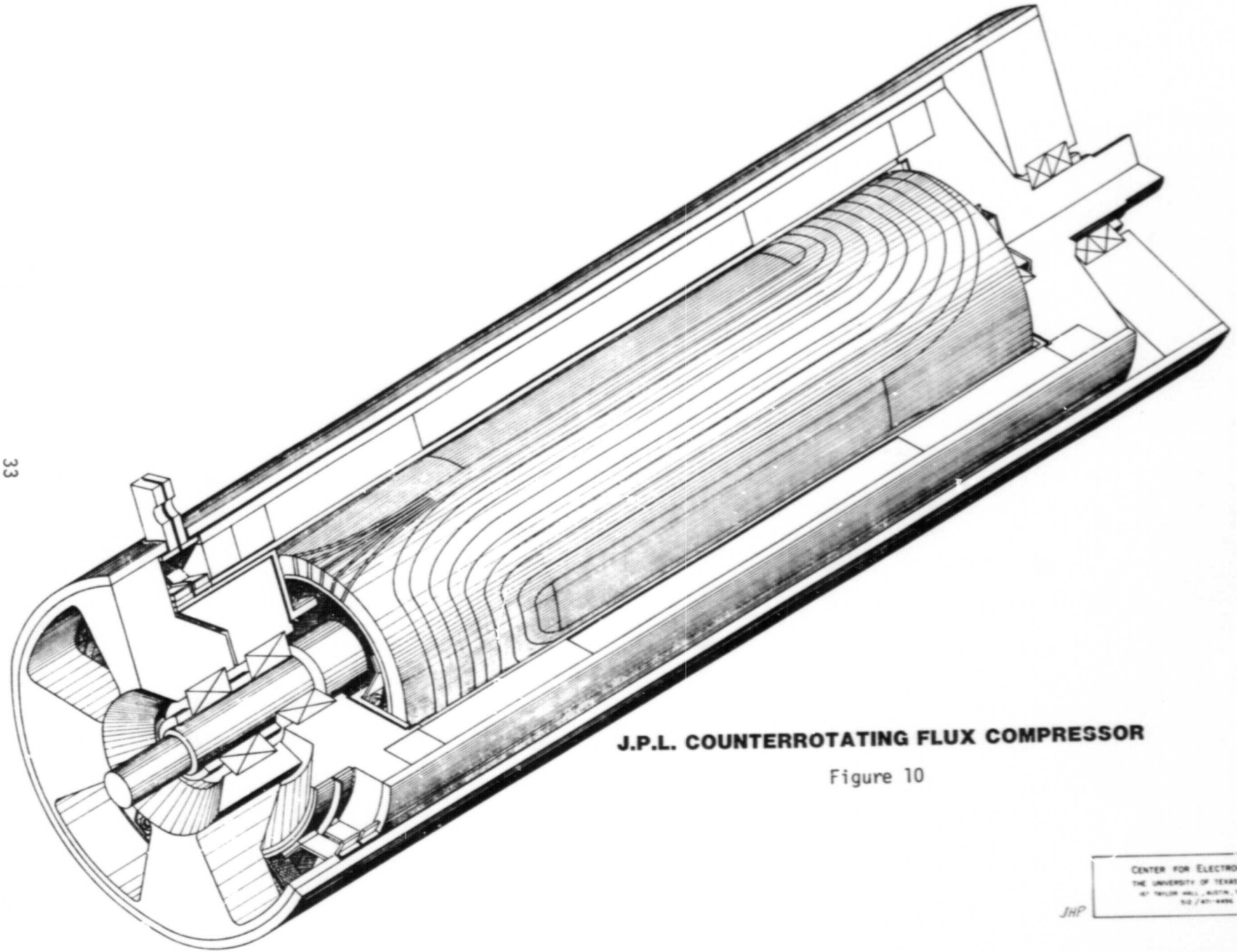

J.P.L. COUNTERROTATING FLUX COMPRESSOR

Figure 10

CENTER FOR ELECTROMECHANICS
THE UNIVERSITY OF TEXAS AT AUSTIN
[illegible] AUSTIN, TEXAS 78712
512 / 471-[illegible]

JHP

DESIGN OF A CARFC TO DRIVE A FLASH LAMP LOAD

Discussion

It is important to preface this section of the report with an explanation of the design history of the machine selected to drive a pulsed laser for space application. At the time of the March 10 meeting between CEM-UT and Ross Jones of JPL it was felt that the design goal of the second part of the project would be to match a compulsator to a flash lamp load. The compulsator would be counterrotating for torque compensation and the flash lamps pumping the laser would be pulsed at 10-20 Hz with 5-10 pulses per burst.

In the June-July progress report a compulsator design was reported. CEM-UT has designed, built, and tested four machines in the compulsator family. The compulsator, the desk model compulsator, the brushless rotary flux compressor, and the active rotary flux compressor (ARFC) all have stationary compensating windings. In order to make use of existing circuit codes half the moment of inertia of the armature drum was spun twice as fast to simulate counterrotation. This technique is suitable for a counterrotating active rotary flux compressor (CARFC) and will be developed later in the report. Unfortunately, in a compulsator where a field winding is required, relative motion between the compensating winding and field winding as well as motion between armature winding and field winding must be addressed. The circuit analysis codes were rewritten in early August and the results showed:

1. the field winding experienced an uncompensated torque, and
2. the percentage of stored energy removed from the hollow shell rotors in one discharge was so great that repetitive pulses could not be taken from the machine.

With this development it was apparent that the iron in the machine would have to be rotated in order to increase the stored energy. This pointed to a CARFC design. The remainder of the report describes the design and operating mode for the JPL CARFC.

The operation of a compulsator involves a number of phenomena, the most important of which are

1. The generation of voltage by the motion of an armature coil through field winding produced flux.

2. The delivery of output current through a circuit of varying inductance that provides:
   a. compensation to reduce inductive impedance to current flow, and
   b. flux compression by changing inductance to enhance output voltage.

A CARFC does not make use of passing the armature coil through field winding produced flux. Current is delivered to the armature and compensating coils from a start-up capacitor. The energy delivered by the external capacitor is then amplified by flux compression. The inertial energy stored in the rotating stator and armature are converted to electrical energy which in turn is delivered to the load through the discharge circuitry. A simplified circuit schematic is presented in Figure 11.

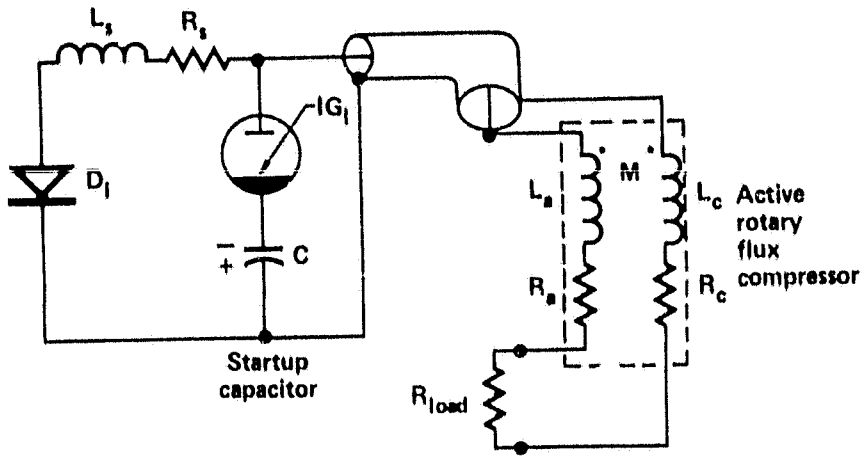

Fig. 11. Simplified CARFC Circuit Diagram

The mode of operation for the CARFC will require recharging the start-up capacitor in a pulsed mode. Presently the design uses a 400-μF, 5-kJ capacitor to start current in the machine. The 20 Hz operation requires the second pulse 50 ms later. Therefore if the capacitor is pulse-charged from the 100 kW prime power source, this mode of operation will provide the desired burst. It is appropriate to mention at this point that five to ten 50-kJ capacitor banks would be required to duplicate the pulsed discharge. A 100-kW supply cannot pulse charge a single 50-kJ bank to provide a 20-Hz burst.

CARFC Description

The JPL CARFC is shown in Figure 12. The flux compressor has three main mechanical parts:

1. nonrotating shell and bearing structure,
2. the rotating stator member,* and
3. the rotor member.

This machine is required to store a relatively large amount of energy so that the last of the multiple pulses may be delivered with pulse width short enough to maintain maximum laser gain. For this reason the speed of the stator is established by the endurance limit of the sheet steel used in making the laminations. The next consideration is the flux compression ratio that will determine energy gain through the system. The configuration of the winding on the rotor and stator determine this variation. A compensating winding is connected in series opposition to the armature winding to confine the armature flux at peak current between the windings. The armature winding and compensating winding are bonded to smooth steel surfaces of the rotor and stator respectively. The conductors are not embedded in slots, thereby eliminating slot leakage reactance. Finally, the conductors are made radially thin so that the windings approach the low inductance form of cylindrical current sheets.

The penalty for designing the machine in this manner is that the armature conductors are exposed to the full air gap flux. Therefore the full energy conversion forces are developed at the conductor and not on iron teeth. Since the moment of inertia of the conductors is a small fraction of the total inertia of the rotor, this force must be transmitted by the electrical insulation system in shear. In addition the armature conductors must be finely stranded and transposed to reduce open circuit eddy current losses. [17]

---

*This is a misnomer in that the stator rotates in this machine. If the counterrotating winding is pinned to the support structure, then this component resembles the stator in the CEM-UT ARFC. Therefore it will be described as the stator.

Figure 12

J.P.L. COUNTERROTATING FLUX COMPRESSOR

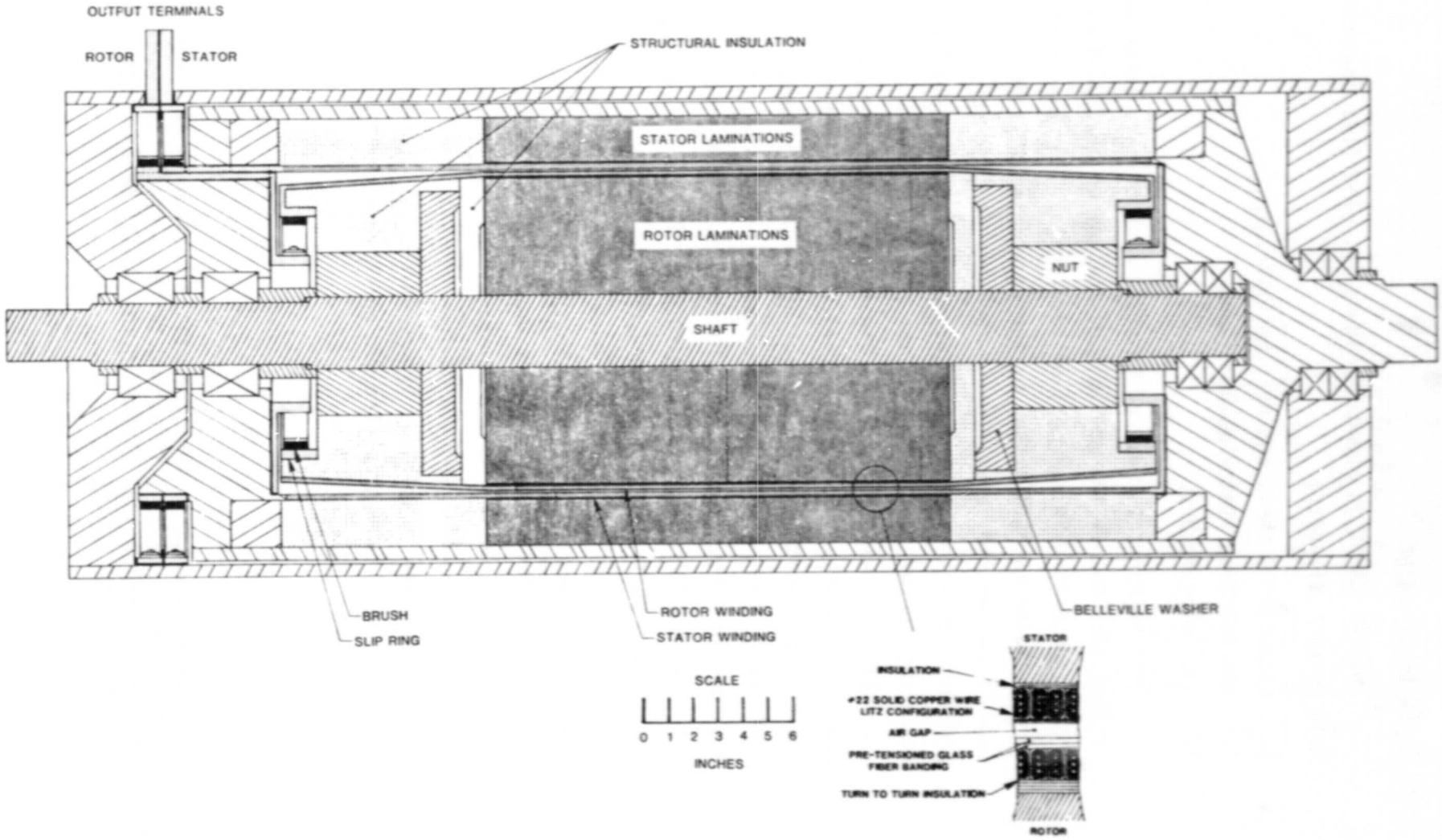

Discharge current is transferred from one rotating member to the next through slip rings and brush mechanisms. Careful attention must be given to insulation design. Tracking paths must be made physically long and corona suppression must be designed for the air gap insulation.

The prime movers are the final members of the system. They are attached to the fixed shell structures and accelerate the inertias of the rotor and stator to design speed in a counterrotating mode.

CARFC Load

The load for the CARFC consists of six Xenon flash lamps in parallel pumping an Nd glass laser. In order to produce a 1,000-J pulse from the laser the delivered energy to the flash lamp load will have to be 50 kJ (assuming a 2% laser efficiency).

The load parameters are as listed below:

Number of load circuits	6
Final diameter of arc (m)	0.015
Length (m)	0.746
Initial diameter of arc (m)	0.00015
Lamp pressure (torr)	300

Mechanical Design

The first design consideration was to set the rotor diameter. To do this the prototype compulsator and ARFC built at CEM-UT were examined (Table 5). In the repetitive discharge mode it will be necessary to store enough energy that the rotor maintains sufficient speed to provide an appropriately short pulse width for the last pulse in the burst. We will be removing over 50 kJ per discharge. For this reason a diameter closer to the compulsator diameter will be selected.

Stator Design. The diameter of the rotor will be set at 0.304 m. From flux path considerations the outer radius of the stator is described by

$$\frac{2\pi r_s}{2N_p} = r_s' - r_s$$

r_s = stator inner radius
r_s' = stator outer radius
N_p = no. of poles.

With both the stator and rotor spinning the machine will have a high relative angular velocity and pulse width should not be a problem. Therefore the number of poles will be held at four as in past machines. The outer radius of the stator is selected to be 0.216 m.

The stator tip speed is based on the mechanical stress level in M-19 electrical sheet steel, which is high resistivity, low hysteretic loss material used in conventional generators. M-19 electrical sheet steel has the following mechanical properties:

Ultimate tensile strength	$5.03 \times 10^8 \frac{nt}{m^2}$ (73 ksi)
Yield strength	$3.65 \times 10^8 \frac{nt}{m^2}$ (53 ksi)
Estimated endurance limit	$2.55 \times 10^8 \frac{nt}{m^2}$ (37 ksi).

TABLE 6

DESIGN PARAMETERS OF CEM-UT PROTOTYPE COMPULSATOR AND ARFC

	CEM-UT PROTOTYPE COMPULSATOR	CEM-UT ARFC
No. of poles	4	4
Rotational speed	5,400 rpm	5,600 rpm
Energy stored	3.5 MJ	67 kJ
Rotor diameter	0.401 m	0.2 m
Rotor length	1.22 m	0.406 m
Inductance variation	7:1	46:1

This lamination stock may be chemically treated to provide the desired interlaminar insulation resistance.

The tangential spin stress of a disk with a central hole is given by

$$\sigma_t = \rho v^2 \left(\frac{3+\mu}{8}\right) \left[2 + \left(\frac{r_i}{r_o}\right)^2 \left(1 - \frac{1+3\mu}{3+\mu}\right)\right] \text{ N/m}^2$$

where

ρ = mass density (kg/m^3)
v = tip speed (m/s)
μ = Poisson's ratio (~0.3)
r_i = inner radius (m)
r_o = outer radius (m) .

Using $\rho = 7{,}650 \frac{kg}{m^3}$, $r_i = 0.1625$ m, and $r_o = 0.216$ m, the allowed tip speed is 189 m/s. Allowing a factor of safety of 1.25, the surface speed for this design will be 150 m/s.

The stator will be constructed by stacking the 14-mil-thick laminations to the desired stator length. A 1/2-in 4340 steel tube will slide over the stack. The stack will then be compressed and 2-in-thick 4340 steel washers will be welded in the ends of the tube to hold the stack in compression. In designing the prototype compulsator it was found that a lamination loading of 2.67×10^6 nt (600,000 lbf) would supply an effective Young's modulus of 1.88×10^{10} nt/m^2 (2.72×10^6 psi). At this loading the stress in the tube is 1.52×10^8 nt/m^2 (22,000 psi). The weld is capable of constraining twice the required load.

The angular velocity is

$$\omega = \frac{v}{r_o} = \frac{150 \text{ m/s}}{0.216 \text{ m}} = 694 \text{ rad/s} .$$

The mass as a function of length is

$$m = 623.3 \text{ kg/m } \ell .$$

The required stiffness is then

$$k \geq \omega^2 m$$

$$\geq 3.01 \times 10^8 \frac{nt}{m^2} \ell \ .$$

When this expression is related to the stiffness of the structure

$$k = \frac{384\ EI}{5\ell^3}$$

an expression for the allowed length results and that length is found to be

$$\ell < 2.19 \text{ m} \ .$$

The length of the stator will be set at 1.07 m. Of this length several inches at either end of the lamination stack will be replaced with a G-10 spacer on which to wind the stator end turns. This will help to reduce the circuit eddy current resistance.

The lamination length in the stator will be 0.471 m. The moment of inertia of the stator assembly is 15.97 J-s^2. The mass of the stator is 389.6 kg.

Rotor Design. The lamination length in the rotor will match the lamination length in the stator.

As shown in Figure 13 the rotor was treated as a simple supported beam with varying material properties and cross sections. Solving the above system yields the stiffness

$$K_{rotor} = \left[\frac{5b^3}{384\ E_1 I_1} + \frac{5b^2 a}{48\ E_1 I_1} + \frac{ba^2}{4\ E_1 I_1} + \frac{a^3}{6\ E_2 I_2} \right]^{-1}$$

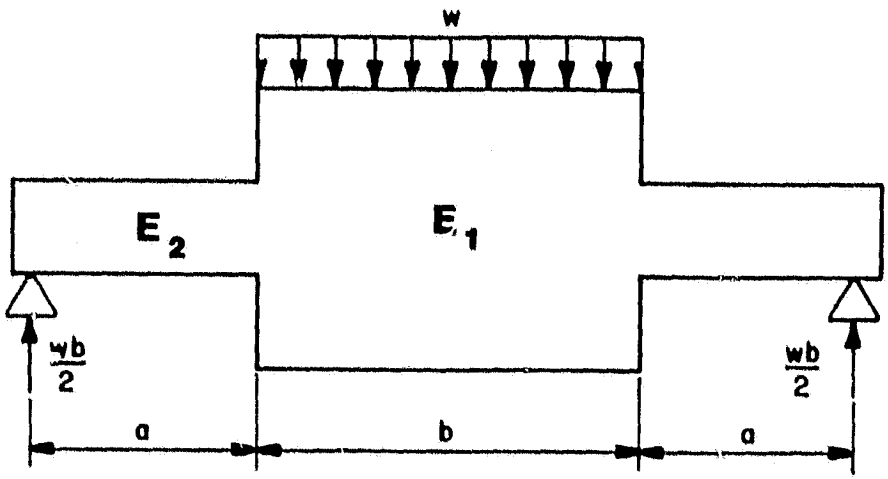

Fig. 13. Model of Laminated Rotor

The rotor mass is 326 kg.

$$\omega_{crit} = \sqrt{\frac{k}{m}} = 812 \text{ rad/s} .$$

This calculation shows that the rotor may spin at the same angular velocity as the stator assuming the bearing and support structure can be designed with its critical frequency above the operating speed.

The rotor is assembled by shrinking a 4340 steel shaft in the lamination stack. Next the laminations are preferentially loaded at their outer radius by using large nuts to compress Belleville washers made of 4140 steel. G-10 structural insulation is then placed over the nut and washer to provide a surface on which to wind the end turns.

Mechanical Structure

The dynamic model for the machine structure is presented in Figure 14. The stator stiffness is calculated to be 6.44×10^9 nt/m and is neglected in the model. The values of the other stiffnesses are given in the figure. When this model is analyzed, the first mode critical frequency where the rotor mass and stator mass are vibrating in phase is 9,292 rpm. The second mode critical frequency where the rotor and stator mass are vibrating 180° out of phase is 19,900 rpm. The first mode can be excited because the relative speed between the rotor and stator is 12,000 rpm. If k_6, the mount stiffness, is made small, the first mode critical is reduced to 8 rpm and the second mode is at 13,500 rpm. The machine will therefore be mounted on soft supports and the first critical will be run through at a low speed. The operating speed of the machine is below the second critical.

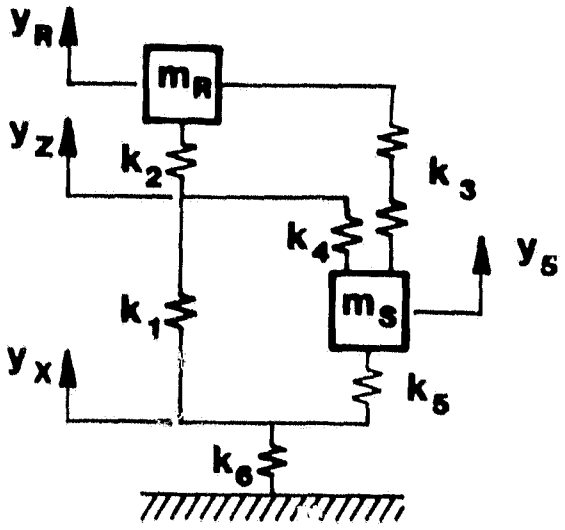

K_1	=	bearing stiffness	8.76×10^8 nt/m
K_2	=	rotor stiffness	2.15×10^8 nt/m
k_3	=	series combination of the bearing stiffness and the rotor stiffness	1.73×10^8 nt/m
K_4	=	bearing stiffness	8.76×10^8 nt/m
K_5	=	bearing stiffness	8.76×10^8 nt/m
K_6	=	mount stiffness	5.25×10^9 nt/m

Fig. 14. CARFC Lumped Mass Dynamic Model

Winding Configuration

Both the armature winding and the compensating winding are located in the magnetic air gap between the rotor periphery and the stator bore. The conductors are not imbedded in slots, but are held in place by the adhesive bond formed by the ground plane insulation (glass filled epoxy) and the steel rotor or stator. The air gap configuration has been proposed for large synchronous generators and has been used for the armature winding of superconducting alternators. The configuration is used in the compulsator to reduce the minimum armature inductance and increase flux compression action to improve machine performance.

To minimize inductance the conductors are radially thin and the radial separation between the rotor winding and stator winding is as small as electrical and mechanical constraints permit. Since the conductors are fully exposed to the applied magnetic field, the mechanical forces on the conductors and insulation are larger than in conventional machinery where the primary forces are exerted on the rotor teeth. Therefore, multilayer windings and windings with crossovers, such as the lap and spiral windings shown in Figure 15 are avoided. A single layer, multiturn wave winding is used. The wave winding is modified to eliminate the crossover by removing one conductor under one pole and using the closely coupled compensating winding as the current return (see Fig. 16). Notice that both windings have one missing conductor and that slip rings are located at both ends of the rotor. [17]

The rotor and stator windings are four poles with 9 turns per pole. Due to the nature of the modified wave winding one pole contains only eight turns making a total of 35 turns. The wire is eight no. 22, solid wires transposed in a Litz configuration. Each turn consists of 13 parallel Litz wires. The insulation build-up and conductor spacing through the air gap is shown in the exploded view in Figure 12.

Electrical Insulation

The short time dielectric strength of the fiberglass reinforced epoxy insulation system is about 450-500 VPM. Generally, the manufacturers dictate the rating for continuous operation and long life to 40 VPM due to effects of corona and temperature, and to allow for transient voltage surges. The ARFC will see a 2.0 per unit switching surge during start-up due to pulse charging of interwinding capacitance by the start-up capacitor. In addition, during the main pulse, there is a potential for peak voltages larger than the start-up voltage if the distributing L di/dt and i dL/at are skewed. If the armature and compensating winding voltage proves to be uniformly distributed, it may be permissible to increase the dielectric stress to greater than 100 VPM peak. Mica paper insulation is used for the air gap insulation since it is not required to transmit torque and is more resistive to corona. The mica paper is generally supplied with a fiberglass reinforced epoxy backing. Although it is more resistant

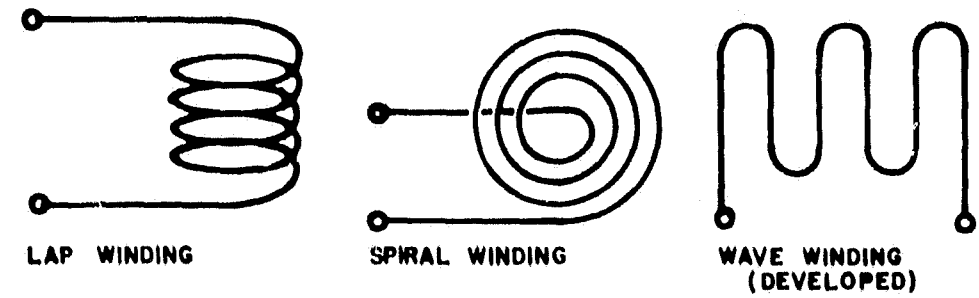

Fig. 15. Conventional Armature Windings

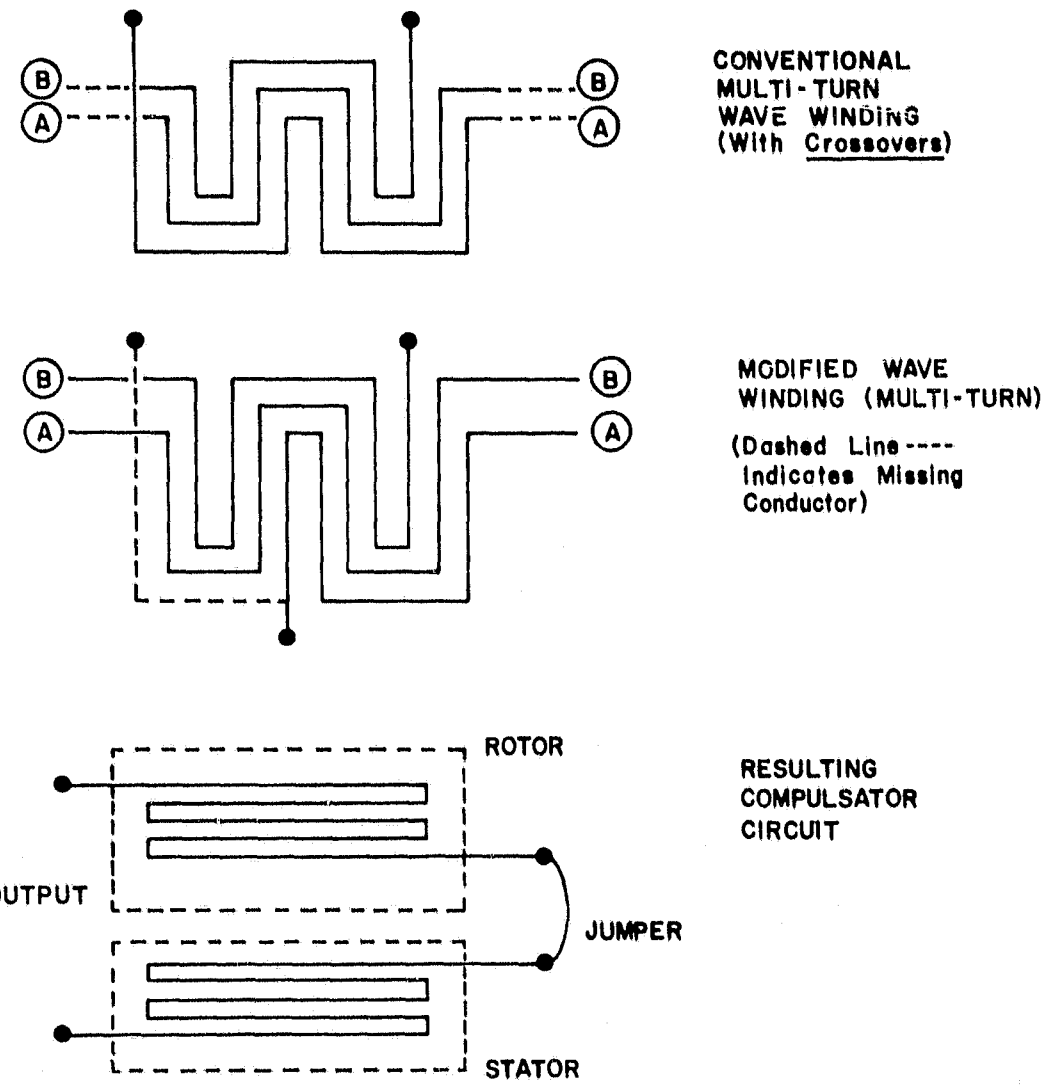

Fig. 16. Modified Wave Winding

to the effects of corona, it does have a smaller short time dielectric strength.

The performance of the generator can be improved if the insulation is stressed to higher levels. The minimum inductance and unsaturated flux compression ratios are sensitive to variations in insulation thickness. However, other limitations such as insulator surface tracking and minimum tape thickness for successful vacuum impregnation should be considered. In addition, constraints such as magnetic saturation and mechanical shear strength practically limit the benefits of reducing the insulation thickness. [18]

Winding Fabrication

Each individual Litz wire is half lap wrapped with 3-mil fiberglass tape. The bundle of 13 wires is then half lap wrapped with 6-mil tape. After preparation for bonding the rotor surface will be half lap wrapped with two layers of 6-mil tape providing a ground plane insulation thickness of 24 mils. The conductors are then wound in the modified wave winding. Once the winding is in place the rotor will be fitted into a closely fitting vacuum vessel. This vessel will register off of the rotor bearing journals and the winding will be vacuum impregnated with a low viscosity epoxy system. The same technique will be employed on the stator system with a recognized greater degree of difficulty. The winding has to be wrapped on a mandrel and then inserted in the stator bore. Next, pressure has to be applied to the winding to force the outer wrap of ground plane insulation against the stator bore. A vacuum must then be applied to the winding to successfully impregnate the winding. The dimensions of the winding are given in Table 6 and are described in Figure 17.

Inductance Calculation

The winding inductance is calculated using a two-dimensional space harmonic distribution code.

Maximum inductance	2,217 μH
Minimum inductance	7.58 μH

TABLE 7

CARFC WINDING DIMENSIONS
(See Figure 16.)

Winding Parameter	Value
R_R	0.1524 m
R_1	0.1535 m
R_2	0.1563 m
R_5	0.1586 m
R_6	0.1614 m
R_S	0.1625 m
β_{2A}	70.84°
β_{1A}	62.97°
γ_{2A}	19.15°
γ_{1A}	23.1 °
β_{2C}	68.52°
β_{1C}	60.92°
γ_{2C}	21.46°
γ_{1C}	25.28°
ℓ_a	0.4714 m
ℓ_c	0.8354 m

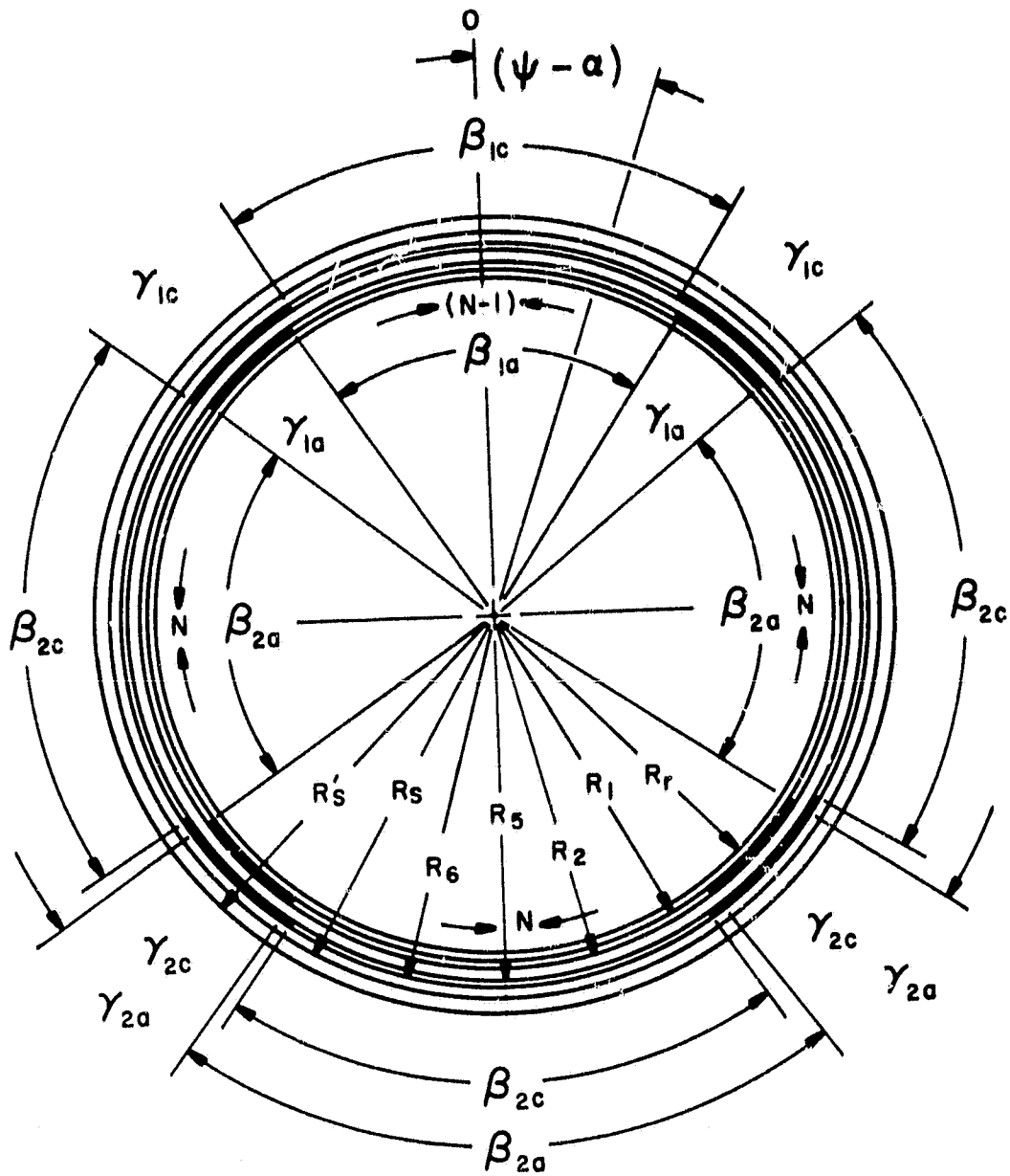

Fig. 17. CARFC Geometry

The unsaturated compression ratio of this design is

$$CR = \frac{2217}{7.58} = 292.5{:}1 \ .$$

Stray Eddy Current Losses

In addition to the winding resistance, other losses must be considered when performing the circuit analysis and designing the machine. Although hysteresis and lamination eddy current losses in the active region of the rotor and stator stack are not significant compared to winding resistance, other stray losses in the end turn region are important.

Measurements of the existing ARFC impedance have shown that the ratio of ac to dc resistance at 1 kHz is 2.7:1. Measurements at higher frequency have indicated that the stray losses in the existing machine scale almost linearly with frequency. Based on this data, the estimated stray loss in the maximum inductance position for this design is 52.7 mΩ. [18]

Magnetic Saturation of Rotor and Stator Laminations

To obtain the flux compression ratio necessary for attractive levels of energy gain, it is mandatory that ferromagnetic rotor and stator boundaries be maintained during the start-up phase of the pulse. As the current increases during flux compression, the uncompensated ampere-turn mmf will be sufficient to drive the laminated material into magnetic saturation at peak magnetic flux densities exceeding 3 T. The resultant decrease in magnetic permeability reduces the magnitude of the inductance early in the pulse, giving an increased pulse width. This effect is incorporated into the circuit simulation by means of a global saturation model. [18]

Circuit Model and Results

In order to simulate the case of a counterrotating compulsator a rotor with half the design moment of inertia was made to rotate at twice the speed of one rotor. This is a realistic model because the inertial energy for the two rotors is

$$1/2\ J_1\omega_1^2 + 1/2\ J_2\omega_2^2 = J_1\omega_1^2$$

$$J_1 = J_2$$

$$\omega_1 = \omega_2 .$$

If a rotor with half the moment of inertia of one rotor is rotated twice as fast,

$$1/2\ (\frac{J_1}{2})\ (2\omega_1)^2 = J_1\omega_1^2$$

the total stored energy is unchanged.

The circuit model and parameter values are given in Figure 18. Table 7 presents a synopsis of output parameters. Figure 19 gives the delivered energy versus time.

TABLE 8
CARFC OUTPUT PARAMETERS

OUTPUT PARAMETER	VALUE
Start-up current (kA)	16.9
Time to crowbar (ms)	0.86
Peak current (kA)	50.5
Time to peak (ms)	1.12
Time to zero amp (ms)	1.58
Maximum load voltage (kV)	5.43
Delivered energy (kJ)	58.3
Energy gain	11.66
Current gain	2.98
Time T2 (upper 1/2 point)(ms)	1.18
Time T1 (lower 1/2 point)(ms)	0.925
Half width (μs)	255
Final speed/initial speed	0.996

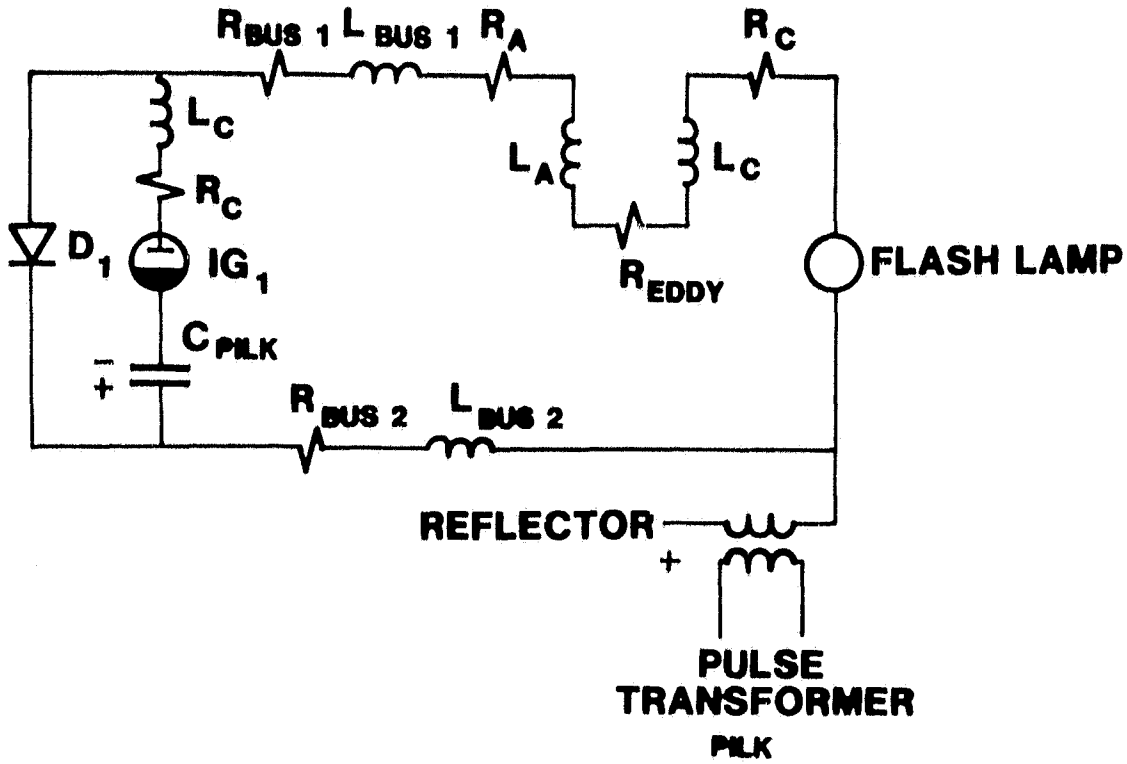

$R_{A20°C} = 14.95 \times 10^{-3}\Omega$

$R_{C20°C} = 14.95 \times 10^{-3}\Omega$

$R_{eddy} = 52.7 \times 10^{-3}\Omega$

$R_{BUS1} = 1.495 \times 10^{-3}\Omega$

$L_{BUS1} = 3.79 \times 10^{-7}H$

$R_{BUS2} = 1.495 \times 10^{-3}\Omega$

$L_{BUS2} = 3.79 \times 10^{-7}H$

$R_c = 1.65 \times 10^{-3}\Omega$

$L_c = 7.24 \times 10^{-7}H$

$C_{pilk} = 400 \times 10^{-6}F$

$V_{pilk} = -5{,}000\ V$

Fig. 18. CARFC Circuit Model and Parameter Values

It can be seen that the machine delivered 58 kJ to the load in a half width time of 255 μs. Only 0.4% of the relative speed between the rotor and stator was lost. Although the code does not have a restart option, it is apparent that the pulse train can be realized. The temperature rise in the winding was only 2°C.

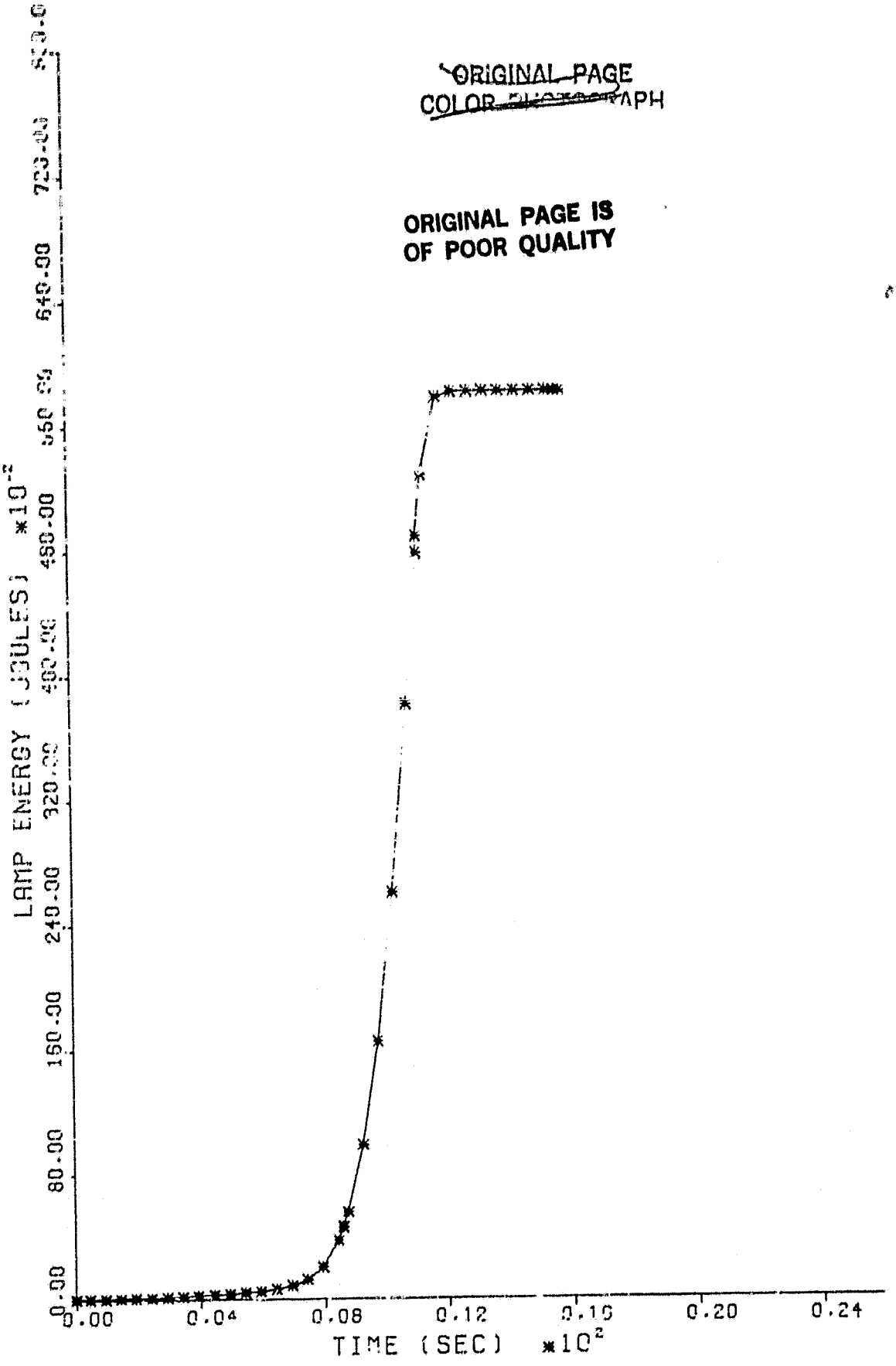

Fig. 19. Delivered Energy vs. Time

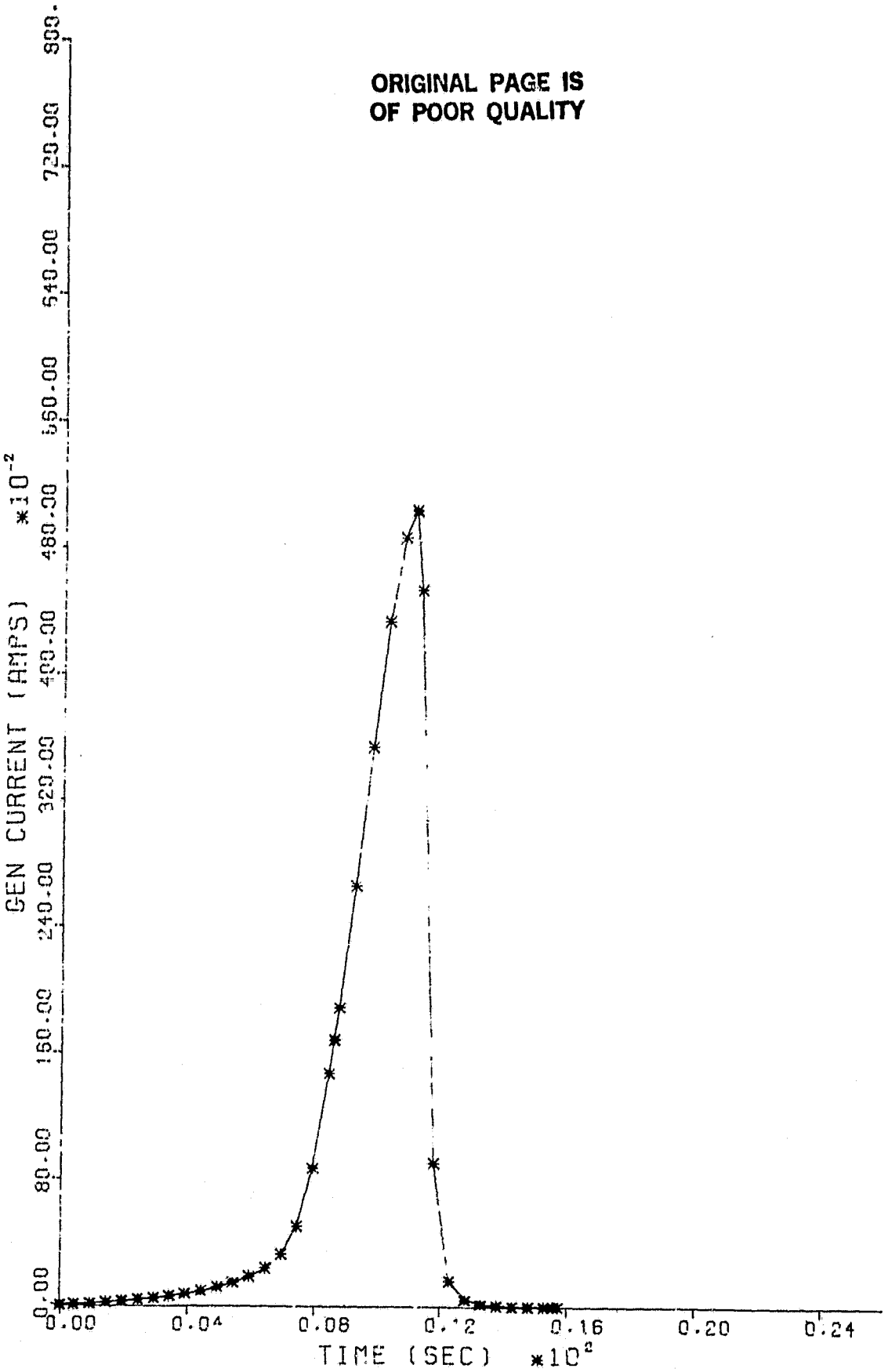

Fig. 20. CARFC Current Waveform

System Weight

Aluminum support structure	163 kg	359 lb_m
Stator	389.6 kg	860 lb_m
Rotor	326 kg	719 lb_m
Prime movers (est.) Disk induction motor	101 kg	220 lb_m
	979.6 kg	2,158 lb_m

System Volume

$$\pi(0.2464\ m)^2(1.27\ m) = 0.24\ m^3\ (8.55\ ft^3)$$

System Cost

Rotor lamination	\$ 7.55/lb	\$5,423
Rotor shaft	\$15.72/lb	\$1,634
Stator lamination	\$ 7.55/lb	\$3,815
Stator tube	\$ 1.50/lb	\$ 447
Support structure	\$ 1.25/lb	\$ 468
Bearings		\$1,000
Brush system	\$50/$in.^2$	\$3,545
Epoxy systems and tape		
Litz wire	\$21.25/lb	\$ 825
Subtotal		\$18,107
Manufacturing cost (est.)		\$36,000
Motoring system (est.)		\$20,000
Controls		\$15,000
		\$89,107

System Life

The present operating mode is understood to be 3 to 4 burst discharges per day. The brushes will deliver 130,000 bursts. If the machine duty increases, temperature rise in the winding conductors will degrade

insulation properties. Otherwise, the machine is not unlike large rotating machinery with 10,000 operating hours between maintenance checks.

Efficiency

The CARFC duty cycle of 3 to 4 burst discharges a day does not warrant a utilization efficiency calculation. Assuming an 85% efficiency of the disk rotor induction motors, the inertia of the flux compressor is brought to speed in 1-1/2 min. The energy stored is 7.7 MJ. Another source of loss will appear in charging the 5-kJ start-up capacitor at the 50-ms intervals. A 95% charging efficiency might be realized. The final operating loss is the bearing, seal, and windage loss. On the prototype compulsator these losses were 35 kW at 5,400 rpm. The circuit losses on discharge are presented:

Circuit Element	Resistive Loss (J)
Armature conductor	6,820
Compensating conductor	6,820
Eddy current losses	712
Bus resistance	1,360

CONCLUSIONS

The JPL homopolar stores 388 kJ of energy in two counterrotating rotors. It delivers 145 kJ to the MPD thruster load in 30 ms. The initial voltage and current are 167 V @ 32 kA. At the end of the pulse, the voltage and current are 167 V @ 32 kA. The stopping torque on one rotor opposes the stopping torque on the second rotor thereby compensating external torque. The field excitation is provided by a superconducting field coil modeled closely after an operational magnet. The estimated heat leak from the coils is 2.25 ℓ/hr and an installed liquifier will be required. The bearing system needs further research. It is felt that the ceramic rolling element bearings are good candidates for running in the high magnetic fields. The brush system must survive 10^7 cycles over a one-year mission. The actuators currently under development at CEM-UT need further testing and evaluation. The graphite fiber-metal matrix brush material shows good wear properties. If it displays the same characteristic as the copper-graphite material (i.e., orders of magnitude lower wear rate for 20 ms cycle times as opposed to 60-s cycle times) then a candidate brush material already exists. The disk rotor induction motors used to motor the HPG will require an inverter powered by the prime power source. This should provide a constant power method for charging the HPG. The weight of the HPG system is 2,133 kg and it occupies approximately 0.5947 m^3.

The JPL CARFC stores 7.7 MJ of energy. It delivers ten 50-kJ, 255-μs pulses at a rep rate of 50 ms (20 Hz) to six parallel Xenon flash lamps pumping an Nd glass laser. The laser efficiency is assumed to be 2%. The machine is constructed with counterrotating members to minimize external reaction torque. The design requires a 5-kJ, 5-kV start-up capacitor to deliver current to the CARFC winding. This capacitor is pulse charged every 50 ms during the burst. The bearings are rolling element steel bearings and will require hydraulic oil cooling at low flow rates.

Further technology is being developed at CEM-UT for vacuum impregnation of rotors and stators in the compulsator family of machines. The machine duty cycle is short and the frequency of operation is small,

therefore the brushes may be left in contact with the slip ring at all times. The energy stored in the CARFC is large. If the rotor speed is lowered, the required 50 kJ per pulse is not realized. If mass is removed from the rotors, there is a greater speed change per pulse. Subsequently, the pulse width on successive pulses increases and lamp gain goes down. As in the HPG design, disk rotor induction motors are presented as possible prime movers. With a temperature rise in the winding of only 2°C per pulse, a burst discharge from the CARFC looks practical.

ACKNOWLEDGMENTS

I would like to thank Mr. Jayesh Parekh for his circuit and parametric analysis for the homopolar generator and the compulsator. Mr. William Bird offered great assistance in adding the code to analyze the counterrotation of compulsators to existing circuit programs. He also provided instruction in the use of all compulsator and flux compressor design programs. Mr. Mark Pichot designed the lumped mass dynamic model for the counterrotating flux compressor and offered insight into the mechanical problems encountered in the homopolar and flux compressor designs. Mr. William Weldon read all reports for technical content, directed the project, and suggested technology capable of realizing bearing systems and motorings systems requirements. Finally, special thanks goes to Mr. John Price for producing the isometrics that give a very good indication of how the machines might actually appear.

REFERENCES

1. Mark A. Pichot, "Design, Construction, and Testing of a Desk Model Compensated Pulsed Alternator," Masters Thesis, University of Texas at Austin, 1980.

2. Robert G. John, "Pulsed Electromagnetic Gass Acceleration," Jet Propulsion Laboratory Contract No. 954997 (March 1979).

3. M. D. Driga, "Fundamental Limitations and Topological Considerations for Fast Discharging Homopolar Machines," IEEE Trans. on Plas. Sci. PS-3 (4) (1975).

4. Energy Storage Group, "Fast Discharging Homopolar Machines for Fusion Devices," Initial Status Report to Los Alamos Scientific Laboratory (May 1975).

5. M. D. Driga, "Fast Discharge Acyclic Machines," Center for Electromechanics, Publication No. PN-13 (April 1975).

6. J. H. Gully et al., "The Design, Construction and Initial Testing of a Fast Discharge Homopolar Generator," Final Report, Electric Power Research Institute Research Project No. 469-3 (December 1976).

7. R. A. Marshall, P. Reichner, and R. M. Shepian, "Current Collection Systems for Pulse Power Homopolar Machines," Proceedings of the Seventh Symposium on Engineering Problems of Fusion Research held at Knoxville, Tennessee (October 1977).

8. K. D. Timmerhaus and D. H. Weitzel, eds., Advances in Cryogenic Engineering, Vol. 21, Proceedings of the First International Cryogenic Materials Conference, Kingston, Ontario, Canada, July 22-25 1975 (New York: Plenum Press, 1977).

9. H. Bruchna, "Superconducting Magnets" in Superconducting Machines and Devices, S. Foner, B. B. Schwartz, eds. (Plenum Press, New York, 1974).

10. R. A. Marshall, "Design of Brush Gear for High Current Pulses and High Rubbing Velocities," IEEE Trans. Power Appar. Syst. PAS-85(11), 1177-1188.

11. J. M. Casstevens, "Measurement of the Friction and Wear Characteristics of Copper-Graphite Sliding Electrical Contact Materials at Very High Speeds and Current Densities," Masters Thesis, The University of Texas at Austin, 1976.

12. Maneck J. Bharucha, "Testing and Evaluation of Brushes Used for Fast Discharge Homopolar Generator through the Use of the Controlled Atmosphere Brush-Testing Facility," Masters Thesis, The University of Texas at Austin, 1978.

13. Cecil H. Ramage, "An Investigation of the Tribological Properties of Graphite Fiber-Metal Matrix Composites," Ph.D. Dissertation, The University of Texas at Austin, 1977.

14. James J. O'Connor and John Boyd, eds., Standard Handbook of Lubrication Engineering (New York: McGraw-Hill Book Company, 1968).

15. Electric Machines and Electromechanics, S. A. Nasar, ed., Vol. 1, No. 1 (December 1976).

16. John W. Lucek and Paul E. Crowley, "Investigation of the Use of Ceramic Material in Aircraft Bearings," Final Report NASC N00019-76-C-0251 (June 1979).

17. William L. Bird, Jr., "Detailed Design, Fabrication and Testing of an Engineering Prototype Compensated Pulsed Alternator," Lawrence Livermore National Laboratory, Purchase Order No. 3325309 (March 1980).

18. William L. Bird, Jr., "Continued Development of Compensated Pulsed Alternators and Rotary Flux Compressors for Pulsed Power Generation," Quarterly Progress Report (1981).